

Observational and model evidence for a prominent stratospheric influence on variability in tropospheric nitrous oxide

Cynthia D. Nevison¹, Qing Liang², Paul A. Newman², Britton B. Stephens³, Geoff Dutton^{4,5}, Xin Lan^{4,5},
Roisin Commane⁶, Yenny Gonzalez^{7,8}, Eric Kort⁹

5

¹Institute for Arctic and Alpine Research, University of Colorado, Boulder, CO, USA

²NASA Goddard Space Flight Center, Greenbelt, MD, USA

³NSF National Center for Atmospheric Research, Boulder, CO, USA

⁴Global Monitoring Laboratory, NOAA Earth System Research Laboratory, Boulder, CO, USA

10 ⁵Cooperative Institute for Research in Environmental Sciences (CIRES), University of Colorado, Boulder, CO, USA

⁶Department of Earth & Environmental Sciences, Lamont-Doherty Earth Observatory, Columbia University, Palisades, NY, USA

⁷CIMEL Electronique, Paris, 75011, France

⁸Izaña Atmospheric Research Center, AEMET, Santa Cruz de Tenerife, 38001, Spain

15 ⁹Department of Climate & Space Sciences & Engineering, University of Michigan, Ann Arbor, MI, USA

Correspondence to: Cynthia D. Nevison (cynthia.nevison@colorado.edu)

Abstract

The literature presents different views on how the stratosphere influences variability in surface nitrous
oxide (N₂O) and on whether that influence is outweighed by surface emission changes driven by the El
Niño Southern Oscillation (ENSO). These questions are investigated using a chemistry-climate model
with a stratospheric N₂O tracer, surface and aircraft-based N₂O measurements, and indices for ENSO,
polar lower stratospheric temperature (PLST), and the stratospheric quasi-biennial oscillation (QBO).
The model simulates well-defined seasonal cycles in tropospheric N₂O that are caused mainly by the
seasonal descent of N₂O-poor stratospheric air in polar regions with subsequent cross-tropopause
transport and mixing. Similar seasonal cycles are identified in recently available N₂O data from
aircraft. A correlation analysis between the N₂O atmospheric growth rate (AGR) anomaly in long-term
surface monitoring data and the ENSO, PLST, and QBO indices reveals hemispheric differences. In the
northern hemisphere, the surface N₂O AGR is negatively correlated with winter (January-March) PLST.
This correlation is consistent with an influence from the Brewer Dobson Circulation, which brings N₂O-
poor air from the middle and upper stratosphere into the lower stratosphere, with associated warming
due to diabatic descent. In the southern hemisphere, the N₂O AGR is better correlated to QBO and
ENSO indices. These different hemispheric influences on the N₂O AGR are consistent with known

atmospheric dynamics and the complex interaction of the QBO with the Brewer Dobson Circulation.

35 More airborne surveys extending to the tropopause, would help elucidate the stratospheric influence on tropospheric N₂O, allowing for better understanding of surface sources.

1. Introduction

Nitrous oxide (N₂O) is a long-lived greenhouse gas with a global warming potential of 265 relative to
40 CO₂ over a 100 year time horizon (*WMO*, 2018). N₂O has an atmospheric lifetime of about 120 years and is destroyed slowly in the stratosphere by both photolysis and oxidation, with a fraction of the oxidation product yielding NO_x, a catalyst of stratospheric ozone destruction (*Crutzen*, 1970; *Ravishankara et al.*, 2009; *Prather et al.*, 2015). N₂O has abundant natural microbial sources in soil, freshwater and oceans, which account for the majority of global emissions, although anthropogenic
45 sources are becoming increasingly important (*Tian et al.*, 2020; *Canadell et al.*, 2021).

The atmospheric N₂O concentration has risen from about ~270 ppb preindustrially to 336 ppb by 2022 (*MacFarling-Meure et al.*, 2006; *Lan et al.*, 2022). This rise has been attributed largely to Haber-Bosch industrial nitrogen (N) fixation to produce agricultural fertilizer, which has increased the substrate
50 available to N cycling microbes (*Park et al.*, 2012). Recent evidence suggests that N₂O is increasing at an accelerating rate in the atmosphere, possibly due to a nonlinear response of microbes to increasing N inputs in intensively fertilized agricultural systems (*Thompson et al.*, 2019; *Liang et al.*, 2022).

High precision measurements of N₂O have revealed interannual variability in its atmospheric growth
55 rate (AGR) and small-amplitude seasonal cycles in the range of 0.4 to 1 ppb (*Nevison et al.*, 2004; 2007; 2011; *Jiang et al.*, 2007; *Thompson et al.*, 2013). Spatial gradients in atmospheric N₂O are also small, e.g., the northern hemisphere (NH) minus southern hemisphere (SH) difference is approximately 1 ppb (*Thompson et al.*, 2014b; *Liang et al.*, 2022). Larger spatial and seasonal signals in atmospheric N₂O have been observed at sites influenced by strong local agricultural or coastal upwelling sources (*Lueker et al.*, 2003; *Nevison et al.*, 2018; *Ganesan et al.*, 2020). However, at sites remote from local sources
60

even variations of 0.2 ppb in estimated background N₂O levels can significantly affect the magnitude of N₂O emissions inferred from atmospheric inversions (*Nevison et al.*, 2018).

A few studies have inferred information about surface biogeochemical sources based on the observed seasonal cycle in atmospheric N₂O at remote monitoring sites. However, these studies have cautioned that the transport of N₂O-poor air from the stratosphere is a major cause of both seasonal and interannual variability in surface N₂O, which complicates the interpretation of surface emission signals (*Nevison et al.*, 2005; 2011; 2012; *Thompson et al.*, 2014b; *Ray et al.*, 2020; *Ruiz et al.*, 2021). Other studies have argued that ENSO cycles are the major driver of interannual variability in tropospheric N₂O (*Ishijima et al.*, 2009; *Thompson et al.*, 2013; *Canadell et al.*, 2021) or that ENSO-driven variability can obscure the influence of the stratosphere in some years (*Ruiz et al.*, 2021). ENSO refers to the periodic oscillation between warm (El Niño) and cold (La Niña) phases in sea surface temperature over the eastern tropical Pacific (ETP). During the El Niño phase, the warming and deepening of the thermocline is associated with reduced upwelling in the ETP and drought in South America, which can decrease oceanic and soil N₂O emissions, respectively (*McPhadden et al.*, 1998; *Ishijima et al.*, 2009; *Babbin et al.*, 2015).

Studies of the stratospheric influence on surface N₂O variability have differed with respect to the relative impact on the NH and SH. *Ray et al.* (2020) found direct correlations between the stratospheric Quasi-Biennial Oscillation (QBO), lagged 8-12 months, and the observed surface N₂O AGR, but in the SH only. The QBO is a tropical, stratospheric, downward-propagating zonal wind variation, with an average period of ~28 months, that dominates the variability of tropical lower stratospheric meteorology (*Baldwin et al.*, 2001; *Butchart*, 2014). *Ruiz et al.* (2021) found a direct correlation between the QBO and N₂O photochemical loss rates in the tropical middle stratosphere but concluded that interannual variability in surface N₂O globally was governed more by changes in the dynamical processes of the lowermost stratosphere. They showed evidence for a coherent influence of cross-tropopause transport on the surface N₂O seasonal cycle in the NH but not the SH.

90 *Nevison et al.* (2011) argued that cross-tropopause transport and mixing drives the N₂O seasonal
minimum in both hemispheres, based on significant correlations between surface N₂O seasonal
anomalies and stratospheric indices reflective of the Brewer-Dobson Circulation (BDC). The BDC is a
planetary-wave-driven, large-scale meridional circulation that transports ozone, greenhouse gases, and
other constituents poleward and maintains the thermal structure of the stratosphere (*Butchart, 2014;*
Minganti et al., 2020). As part of this transport, the BDC brings N₂O-poor air from the tropical middle
95 and upper stratosphere into the polar lower stratosphere in the winter hemisphere (*Liang et al., 2008;*
2009; Nevison et al., 2011).

A better grasp of the controls on tropospheric N₂O variability has important implications for the
interpretation of biogeochemical signals in N₂O data. If abiotic factors associated with the downward
100 transport of N₂O-poor air from the stratosphere contribute significantly to variability, they must be
disentangled from the data before inferring information about surface biogeochemistry and emissions.
Understanding the influence of stratospheric variability on surface N₂O also may provide insight into
anomalous changes in the AGR of CFC-11, which has a stratospheric sink similar to that of N₂O (*Ray et*
al., 2020; Ruiz et al., 2021; Lickley et al., 2021).

105

This paper explores the causes of variability in both the seasonal cycle and the AGR of tropospheric
N₂O. It follows up on previous work by *Nevison et al.* (2011), who inferred a stratospheric influence in
surface atmospheric N₂O data based entirely on correlations between interannual variations in
stratospheric indices and detrended N₂O anomalies in months surrounding the seasonal N₂O minimum.
110 In the meantime, observed altitude-latitude cross sections have become available from aircraft surveys
that span a full seasonal cycle. In addition, advances in model development allow for explicit
simulation of stratospheric N₂O tracers (*Ruiz et al., 2021; Liang et al., 2022*).

This study uses the NASA Goddard GEOS-5 Chemistry-Climate Model (GEOSCCM), which includes a
115 tagged stratospheric N₂O tracer that is transported individually in the model and can be distinguished
from tropospheric tracers of fresh surface emissions (*Liang et al., 2022*). The study also examines

atmospheric N₂O data collected in the NH by the National Oceanic Atmospheric Administration (NOAA) during routine aircraft monitoring, as well as N₂O data measured by recent global airborne surveys spanning both hemispheres. Finally, it performs an updated correlation analysis of surface N₂O anomalies from ground-based NOAA sites against ENSO and QBO indices as well as polar lower stratospheric temperature (PLST), which is used as a tracer for the BDC, with the assumption that significant correlations provide support (although not proof) for causation.

The paper is organized as follows: Section 2 describes the data and methods used. Section 3 presents the results, beginning in Section 3.1 with an examination of climatological mean seasonal cycles and latitude-altitude cross sections of N₂O from GEOSCCM and aircraft data. Section 3.2 examines correlations between variability in the N₂O AGR from NOAA long-term surface monitoring data, PLST, and indices of QBO and ENSO. Section 3.3 examines correlations between PLST and variability in monthly N₂O anomalies near the month of seasonal minimum. Sections 3.2 and 3.3 include parallel correlation analyses of variability in GEOSCCM N₂O sampled at NOAA surface sites and GEOSCCM-based QBO and PLST indices. Section 4 interprets and discusses the results. Section 5 finishes with a summary and future outlook.

2. Methods

2.1 GEOSCCM with tagged stratospheric tracers

GEOSCCM was used to simulate atmospheric N₂O with geographically resolved surface emissions from soil, ocean and anthropogenic sources, and full stratospheric chemistry with stratospheric N₂O destruction due to photolysis and O(¹D) oxidation (*Nielsen et al., 2017; Liang et al., 2022*). GEOSCCM has been evaluated extensively in multi-model assessments and shown to represent well the mean atmospheric circulation, the interhemispheric exchange rate, the mean age of air in the tropical and polar stratosphere, and the mean atmospheric lifetime of N₂O (*Liang et al., 2022* and references therein). For the current study, GEOSCCM was run at 1°x1° resolution with 72 vertical layers from the surface to 0.01 hPa. In addition to the standard total N₂O tracer, four additional N₂O tracers were included to track: 1) aged air from the stratosphere (N₂O_{ST}), and 2) soil, 3) ocean, and 4) anthropogenic

sources freshly emitted in the troposphere. Following the approach of *Liang et al.* (2008), the
145 tropospheric tracers become the stratospheric tracer, N_2O_{ST} , when they are transported across the
tropopause, and retain that identity even when N_2O_{ST} re-enters the troposphere, thereby providing a
model estimate of the stratospheric influence on tropospheric N_2O .

The full GEOSCCM simulation spanned 1980-2019, but this study focuses on the final 20 years from
2000-2019 for the correlation analysis between model surface N_2O anomalies and QBO and PLST. As
150 described in detail in *Liang et al.* (2022), the GEOSCCM N_2O lifetime decreased slightly after 2000
(from 119 ± 2 yr in the 1990s down to 116 ± 2 yr in the 2010s) and model emissions were optimized to
account for the observed change in the atmospheric N_2O growth rate. GEOSCCM temperature and
QBO do not necessarily correspond to observations since both are internally generated by the GEOS
general circulation model, which is free running rather than forced by a reanalysis meteorology.
155 GEOSCCM QBO and PLST were computed in the same way as the observed indices, as described
below in Section 2.4.1 and 2.4.2, respectively. The GEOSCCM N_2O fields were saved as monthly
means and were detrended and converted to anomalies by subtracting a deseasonalized fit to the model
time series sampled at Mauna Loa (MLO). The N_2O time series at MLO is a good proxy for the global
 N_2O trend and thus its subtraction provides a convenient, single-station approach for calculating
160 anomalies of the N_2O mixing ratio for contour plots.

2.2 N_2O Data

2.2.1 Surface N_2O from NOAA long-term monitoring sites

Surface atmospheric N_2O data were obtained from the NOAA Global Monitoring Laboratory (GML)
for comparison to GEOSCCM output. NOAA has two programs that measure N_2O , Halocarbons and
165 other Atmospheric Trace Species (HATS, *Thompson et al.*, 2004) and the Carbon Cycle Greenhouse
Gases group (CCGG, *Lan et al.*, 2022). HATS provides *in situ* data measured every ~ 60 minutes using
the Chromatograph for Atmospheric Trace Species (CATS) instruments at 5 baseline sites (Barrow,
Alaska; Niwot Ridge, Colorado; Mauna Loa, Hawaii; Cape Grim, Tasmania; and South Pole,
Antarctica). CCGG maintains a flask-air sampling network at ~ 55 widely distributed surface sampling

170 sites, in which duplicate samples are collected about weekly and shipped to Boulder, Colorado for
analysis by gas chromatography (GC) with electron capture detection and by a Tunable Infrared Laser
Direct Absorption Spectroscopy (TILDAS) after August, 2019. The instruments are calibrated with a
suite of standards on the WMO X2006A scale maintained by NOAA GML (*Hall et al.*, 2007).
Uncertainties of the measurements (68% confidence interval) range from 0.26 to 0.43 ppb with GC-
175 ECD and 0.16 ppb with TILDAS. The mean uncertainties in CATS GC data are 0.2 to 1.2 ppb (68%
confidence interval) over most of the 2000s, with an increase in recent years as the instruments age.

This study used the NOAA combined HATS/CCGG N₂O product from 1998-2021, which is based on
monthly medians from the CATS *in situ* program (at the 5 HATS baseline sites) and monthly means
180 from the CCGG flask program at a selected subset of 12 of the ~55 total sites
(<https://doi.org/10.15138/GMZ7-2Q16>; *Hall et al.*, 2007). All of the NOAA sites considered in this
study are long-standing remote sites situated away from strong local anthropogenic sources. They
include Alert, Canada; Summit, Greenland; Mace Head, Ireland; Trinidad Head, California, Cape
Kumakahi, Hawaii, Cape Matatula, Samoa; Palmer Station, Antarctica and the 5 HATS baseline sites
185 (at which CCGG also makes overlapping flask measurements). In addition to these 12 individual sites,
global, NH and SH means are estimated from the latitude-binned and mass-weighted means of the
combined monthly means for the 12 sites (*Hall et al.*, 2011). The combined monthly data are first
aggregated at the measurement program level for each sampling location. At sites where both HATS
and CCGG measure, a weighted mean is calculated based on the programs' monthly uncertainties.

190 **2.2.2 NOAA empirical background for atmospheric N₂O**

The NOAA empirical background is a 4-dimensional (4-D) field, constructed from NOAA surface and
aircraft N₂O data, which is used in North American regional inversions to represent the background
concentration of atmospheric N₂O prior to the influence of continental surface fluxes (*Nevison et al.*,
2018). The 4-D field is defined daily over North America from 500-7500 m every 1000 m, from 170°-
195 50°W every 10° longitude, and from 20-70°N every 5° latitude (or, prior to 2017, from 20-80°N every
10° latitude). For this study, a deseasonalized fit to the NOAA time series at Mauna Loa was used to

detrend and remove the mean value (centered in the mid troposphere) of the empirical background data, thus allowing them to be collapsed into a single climatological year and presented as anomalies. The climatology encompassed January 1, 2005-December 31, 2013, a period when atmospheric N₂O was increasing by about 0.9 ppb/yr.

2.2.3 N₂O data from global airborne surveys

Atmospheric N₂O measurements were made *in situ* with the Harvard/Aerodyne Quantum Cascade Laser Spectrometer (QCLS) on three different aircraft campaigns designed to study the atmospheric profiles of greenhouse and related gases (*Wofsy et al.*, 2011; *Stephens et al.*, 2018). QCLS N₂O data are retrieved at 1-Hz with 1s precision of 0.09 ppb and reproducibility with respect to the WMO N₂O scale of 0.2 ppb (*Kort et al.*, 2011; *Santoni et al.*, 2014) on the NOAA-2006 scale (*Hall et al.*, 2007). The first of the campaigns, the High-performance Instrumented Airborne Platform for Environmental Research (HIAPER) Pole to Pole Observations (HIPPO) project, consisted of 5 roughly month-long sets of flights centered over the central Pacific Ocean extending from the surface to the upper troposphere/lower stratosphere and nearly pole to pole (*Wofsy et al.*, 2011). The flights were timed between January 2009 and November 2011 to create a climatological seasonal cycle. The second campaign, O₂/N₂ Ratio and CO₂ Airborne Southern Ocean (ORCAS), took place in January-February 2016 and focused on the Southern Ocean south of ~35°S (*Stephens et al.*, 2018). Most recently, the Atmospheric Tomography Mission (ATom) campaign extended nearly pole to pole over both the Pacific and Atlantic Oceans. ATom consisted of 4 deployments over 3 years, with each deployment approximately 1 month long (*Thompson et al.*, 2022). QCLS N₂O was measured during the second through fourth ATom deployments in January/February 2017, September/October, 2017 and April/May 2018, respectively, but N₂O measurements are not available from the first ATom deployment in July/August 2016 due to technical problems (*Gonzalez et al.*, 2021). For all figures presented below using QCLS N₂O, the flight track data were interpolated onto a 5 degree latitude by 50 hPa grid using the akima package in R (Akima, 1978). In addition, a deseasonalized fit to the NOAA time series at Mauna Loa was subtracted from all data, allowing them to be collapsed into a climatological year and expressed as anomalies.

2.3 Mean seasonal cycles and interannual variability in surface N₂O

225 Mean seasonal cycles for NOAA surface N₂O observations and GEOSCCM N₂O tracers were estimated using a bootstrapping method in which 20% of the timeseries was randomly removed and the remaining 80% was fit to a 3rd order polynomial plus first 4 harmonics. These steps were repeated over 500 iterations to estimate the range of uncertainty in the harmonic components of the fit.

230 Interannual variability in the atmospheric growth rate of N₂O in the NOAA surface NH, SH and global time series was calculated by first removing the seasonal cycle from the monthly mean time series by computing a 12-month running average,

$$X_i = (C_{i-6} + 2 \sum_{k=i-5}^{i+5} C_k + C_{i+6})/24, \quad (1)$$

235 where C is the original monthly mean time series and X is the deseasonalized time series. The slope of the deseasonalized time series then was computed as a central difference,

$$S_i = 12 \frac{x_{i+1} - x_{i-1}}{2}, \quad (2)$$

where S is the centrally differenced slope and the scalar 12 converts S from units of ppb/month to
240 ppb/yr. To account for the increasing growth rate of atmospheric N₂O, the absolute slopes S were converted to atmospheric growth rate anomalies by removing an optimal (increasing) linear fit determined by recursive least squares regression.

Interannual anomalies in the magnitude of the seasonal minimum were calculated by detrending the raw
245 monthly mean N₂O data with a 3rd-order polynomial, after which a climatological seasonal cycle was constructed by taking the average of the detrended data for all Januaries, Februaries, etc. This climatological annual cycle was subtracted from the original raw data to produce a deseasonalized (but not detrended) time series. A running 12-month annual mean of this curve was then computed as in Equation 1, but where C is now the deseasonalized time series rather than the original monthly mean

250 time series. This analysis focused on mid and high latitude sites in the NOAA dataset. At stations with gaps in the monthly data, the original 3rd order polynomial fit was used as a placeholder in the running mean. The running mean was subtracted from the deseasonalized curve to remove the secular trend and other low frequency variability, thus isolating the residual high frequency anomalies.

2.4 Proxies and indices for the correlation analysis

255 The computation of N₂O AGR anomalies from Section 2.3 created a set of monthly-resolved time series for the SH, NH and global means. These were plotted against various proxies and indices for stratospheric influences and ENSO. In addition, the high frequency residuals from Section 2.3 at various mid and high latitude sites were sorted by month and selected months were plotted against PLST as described below in Section 2.4.1. The PLST proxy involves a single value for each year, such
260 that correlation coefficients and p values were computed based on the number of years N with data. For the ENSO and QBO indices, the correlation statistics were computed based on the reduced, effective N (N_{eff}) number of monthly data points after accounting for the autocorrelation that is introduced by the 12-month running mean used to compute the N₂O AGR (see Supplementary text S1 for more details.)

2.4.1 Polar lower stratospheric temperature (PLST) as proxy for the Brewer Dobson Circulation

265 Mean polar (60°-90°) lower stratospheric temperature at 100 hPa in January-March (winter) in the NH and September-November (spring) in the SH was computed from the Modern-Era Retrospective Analysis for Research Applications, Version 2 (MERRA-2) reanalyses (*Gelaro et al., 2017*). The mean PLST in each hemisphere was treated as a proxy for the integrated strength of the BDC, which brings N₂O-poor air from the middle to upper tropical stratosphere into the polar winter lower stratosphere
270 through diabatic descent. PLST represents the cumulative effect of descent throughout fall and winter, with warmer PLST corresponding to stronger descent (*Holton, 2004; Nevison et al., 2007; 2011*). Winter months (January-March) were averaged in the NH and spring months (September-November) in the SH to account for the later seasonal breakup of the Antarctic polar vortex compared to the Arctic polar vortex (*Nevison et al., 2011*). For the monthly analysis, the PLST proxy was regressed against the
275 monthly N₂O anomaly in each of the subsequent months leading up to and encompassing the seasonal

minimum in tropospheric N₂O, which occurs in summer in the NH and autumn in the SH. For the AGR analysis, the mean N₂O AGR anomaly was averaged over 12 months (considering a range of start/end months) for regression against PLST.

2.4.2 Quasi-Biennial Oscillation (QBO)

280 The QBO was quantified using monthly mean stratospheric zonal wind values in m/s derived from twice daily balloon radiosondes conducted by the Meteorological Service Singapore Upper Air Observatory at a station located at 1.34°N, 103.89°E (https://acd-ext.gsfc.nasa.gov/Data_services/met/qbo/QBO_Singapore_Uvals_GSFC.txt). A positive QBO indicates westerly winds and a negative QBO indicates easterly winds. A range of altitudes from 10 mb
285 to 100 mb was considered. Since the QBO index is a monthly mean time series, it can be compared directly to the monthly mean N₂O AGR time series. However, delays are expected between the QBO and its influence on tropospheric N₂O (*Strahan et al.*, 2015; *Ray et al.*, 2020). Therefore, a range of lag times was considered spanning 6-24 months when correlating with the N₂O AGR anomalies to identify the optimal QBO altitude and lag in each hemisphere.

290 2.4.3 ENSO

ENSO cycles were defined using the Niño 3.4 index, which is based on sea surface temperature anomalies from 5°S to 5°N and 170° to 120°W. The Niño 3.4 index defines an El Niño event as a temperature anomaly of > 0.4 °C and a La Niña event as a temperature anomaly of < -0.4 °C. Monthly Niño 3.4 indices were obtained from <https://www.cpc.ncep.noaa.gov/data/indices/sstoi.indices>. Like the
295 QBO index, Niño 3.4 is a monthly time series that can be compared directly to the monthly mean N₂O AGR time series. In the analysis presented here, a range of lag times in the Niño 3.4 index was considered spanning 0-12 months to identify the optimal lag in each hemisphere.

2.5 GEOSCCM correlation analysis

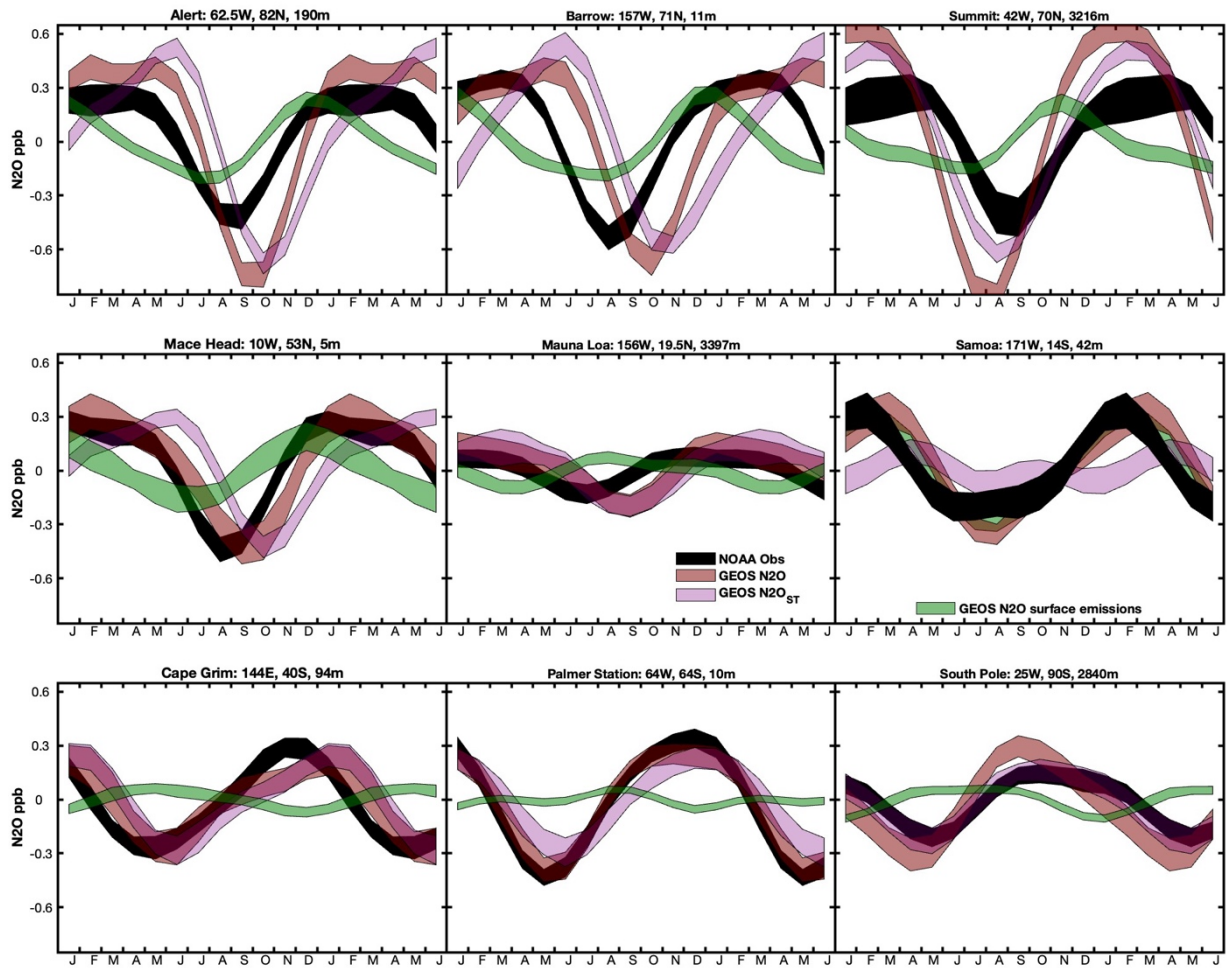
Equations 1 and 2 were applied to GEOSCCM N₂O output sampled at the coordinates of NOAA
300 monitoring sites to create modeled N₂O AGR time series and monthly anomalies, using both total N₂O and N₂O_{ST}. Similarly, mean winter and spring PLST at 100 hPa was calculated for GEOSCCSM

output in the NH and SH, respectively, as described in Section 2.4.1, for each model year from 2000-2019. Finally, a GEOSCCM monthly QBO index was calculated at a range of altitudes from 10 mb to 100 mb by averaging the model zonal wind component in m/s between 5°S and 5°N over each of the 240 months from 2000-2019. A correlation analysis was performed using the GEOSCCM N₂O AGR and monthly anomaly time series regressed against GEOSCCM PLST and QBO, similar to that described for the observed quantities in Sections 2.3-2.4. The ENSO correlation analysis was not applied to GEOSCCM output because the model did not attempt to reproduce the impact of ENSO on surface flux variability (*Liang et al., 2022*).

310 **3. Results**

3.1 Stratospheric influence on tropospheric N₂O in model and aircraft data

Figure 1 shows that the GEOSCCM N₂O mean seasonal cycle at surface sites is dominated by stratospheric air depleted in N₂O that is transported to the surface, rather than by the influence of surface sources. This dominance holds within the uncertainty of the seasonal cycles, as estimated using a bootstrap method. However, the surface emissions tend to pull the total N₂O seasonal minimum about 1 month earlier than the N₂O_{ST} minimum at most sites. Figure 1 also shows that GEOSCCM captures the mean observed seasonal cycle in N₂O relatively well at sites in the SH but overestimates the amplitude of the cycle at sites in the NH, with a ~1-2 month delay in phasing relative to observations.



320 **Figure 1: Detrended seasonal cycles in N_2O mixing ratio (ppb) modeled by GEOSCCM and compared to NOAA**
surface station data at 9 surface sites, with uncertainty estimated using a bootstrap method. Top row from left to
right: Alert (Canada), Barrow (Alaska), Summit (Greenland); middle row from left to right: Mace Head (Ireland),
Mauna Loa (Hawaii), Cape Matatula (Samoa); bottom row from left to right: Cape Grim (Tasmania), Palmer Station
(Antarctica), South Pole (Antarctica). Black is observed N_2O from NOAA. For GEOSCCM, the total N_2O from all
325 forcings is in red and the stratospheric tracer N_2O_{ST} is in magenta. Blue is N_2O due to fresh surface emissions,
representing the combined net influence of the natural soil, ocean, and anthropogenic atmospheric tracers.

Figure 2 provides a two-dimensional view, using zonally-averaged altitude-month contour plots at
 middle and high latitudes in both hemispheres, of how the signal of stratospheric air depleted in N_2O is
 330 transmitted to the surface in GEOSCCM. This N_2O -poor air accumulates during winter (starting in
 ~December in the NH and ~July in the SH) in the polar stratosphere, descends vertically and crosses
 into the troposphere in spring (March-April) in the NH and early summer (January-February) in the SH.

The SH latitude panels in Fig. 2 are plotted with a 6-month shift to help visualize the later seasonal phasing of the stratospheric influence in the SH relative to the NH. After crossing into the troposphere, the N₂O-poor air continues to move downward, and also mixes equatorward, from approximately
 335 the N₂O-poor air continues to move downward, and also mixes equatorward, from approximately January to May at SH mid-to-high latitudes and April to October at NH mid-to-high latitudes (*Liang et al.*, 2009; 2022). Due to lags in downward propagation and mixing, the modeled surface minimum in the lower troposphere does not occur until late summer to early autumn in both hemispheres (Fig. 1 and 2). Supplementary Figure S1 shows a 3-dimensional view of this process in a series of 12 monthly
 340 altitude by latitude plots.

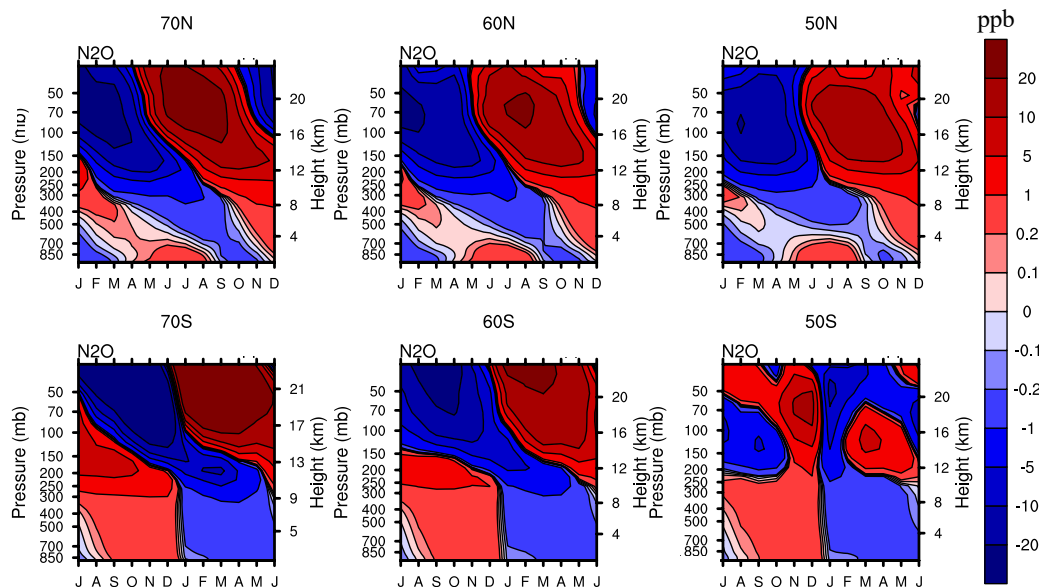
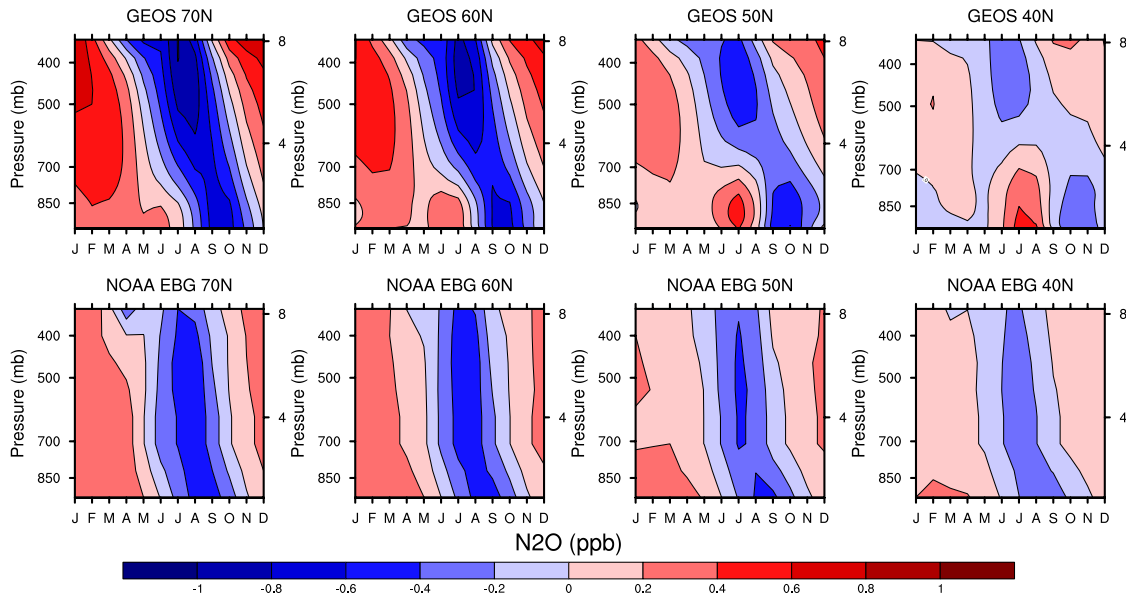


Figure 2: GEOSCCM anomalies of N₂O mixing ratio (ppb) as a function of month and altitude over a mean seasonal cycle, plotted from the surface to 30 hPa in the NH (top row) and SH (bottom row). From left to right: 10° latitude bins centered at 70°, 60° and 50°. Monthly anomalies are computed by subtracting the annual mean value at each pressure level.

345

Figure 3 shows that the NOAA N₂O empirical background, when organized as a series of zonally-averaged altitude-month contour plots at NH latitudes, has features similar to those simulated by GEOSCCM. Both model and observations show a signal of N₂O depletion beginning in early spring in the upper troposphere that propagates down to the surface. In both model and observations, the signal is
 350 strongest at high latitudes and weakens substantially moving equatorward. However, the NOAA data suggest a faster, more direct downward propagation of the stratospheric signal, which arrives at the

surface in August-September, compared to September-October in GEOSCCM. As a result, the phasing of the GEOSCCM surface minimum is delayed ~1-2 months relative to the NOAA empirical background, consistent with the comparison to NOAA surface monitoring data in Fig. 1.



355

Figure 3: Anomalies of N₂O mixing ratio (ppb) as a function of month and altitude over a mean seasonal cycle, plotted from the surface to 8 km (~330 hPa) in the NH for GEOSCCM (top row) and the NOAA empirical background (bottom row). From left to right: 10° latitude bins centered at 70°, 60°, 50° and 40°N. Monthly anomalies are computed by subtracting the annual mean value at each pressure level.

360

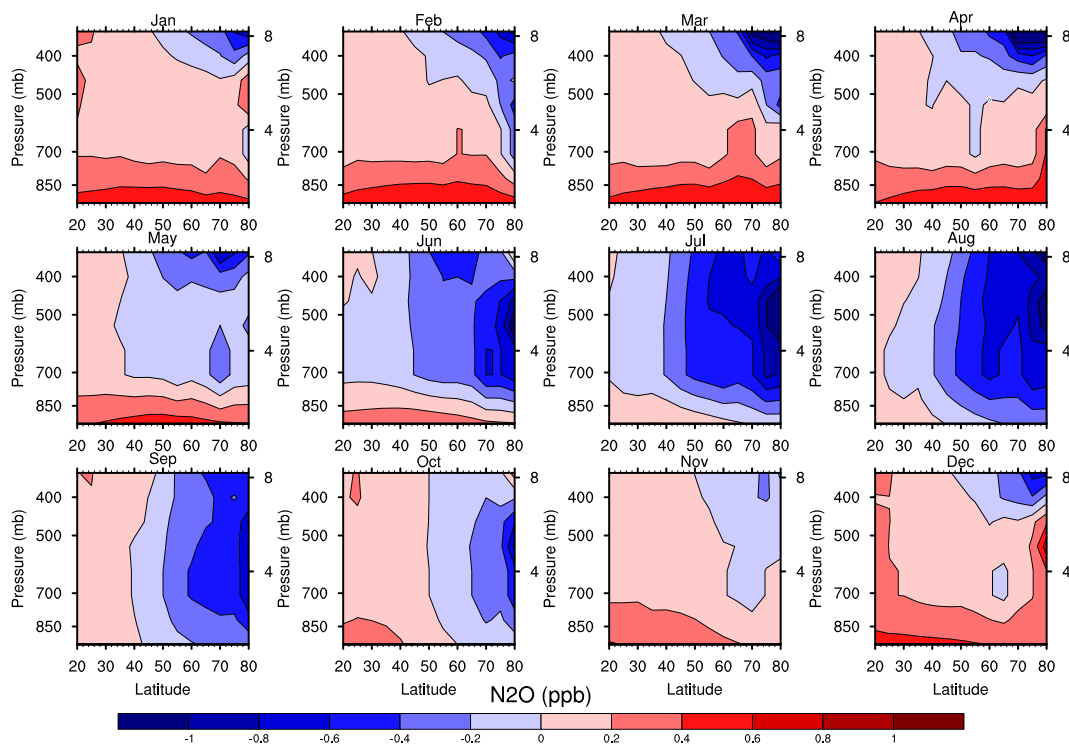
The positive anomalies in Fig. 3 also differ between model and observations, with surface features centered on July at 40°-50°N in GEOSCCM, which uses a summer-dominant soil source (*Liang et al., 2022*), while the NOAA empirical background shows positive surface anomalies in late winter and spring, likely reflecting North American agricultural sources (*Nevison et al., 2018*). At 60° and 70°N, the stronger contrast between positive and negative anomalies throughout the atmospheric column in GEOSCCM compared to NOAA reflects the model's larger seasonal cycle, as seen also in Fig. 1.

365

370

Figure 4 provides a further NH perspective on the signal of N₂O-poor stratospheric air in the NOAA empirical background. When viewed as a 12-month sequence of altitude-latitude contours in the NH, the signal originates at northern polar latitudes in the upper troposphere in late winter and early spring, descends and mixes equatorward, with a peak surface influence around July-September at middle to

high latitudes in the NH that overshadows any surface source signal. By late fall and winter, the signal has dissipated at the surface but is forming again in the upper troposphere.



375

Figure 4: Anomalies of N₂O mixing ratio (ppb) in the NH from the NOAA empirical background, plotted in a monthly sequence of altitude vs. latitude plots extending from the surface up to 8 km (~330 hPa) and from 20°N-80°N.

QCLS N₂O data from airborne surveys extend up to 14 km and thus provide a broader perspective with
 380 respect to altitude of the stratospheric influence on tropospheric N₂O. Of the 3 available airborne
 surveys (HIPPO, ORCAS and ATom), HIPPO provides the most complete N₂O time series across all
 seasons. In Fig. 5, the southbound transects from the five HIPPO deployments are detrended and
 arranged chronologically as altitude-latitude contour plots over an annual mean cycle. These plots form
 a sequence with a similar movement of N₂O-poor stratospheric air from upper levels down to the
 385 surface as seen in GEOSCCM and the NOAA empirical boundary data. This progression is most
 readily seen in the NH in Fig. 5, in which N₂O-poor air in the polar lower stratosphere has crossed the
 tropopause by March. By June it has descended into the middle troposphere and started moving

equatorward, reaching its maximum influence at the surface in August. By October/November, the stratospheric signal is no longer visible at the surface following tropospheric mixing and dilution. This seasonal progression is also evident in a fuller dataset that also includes the ATom and northbound HIPPO transects collapsed into a climatological cycle (Supplementary Fig. S2)

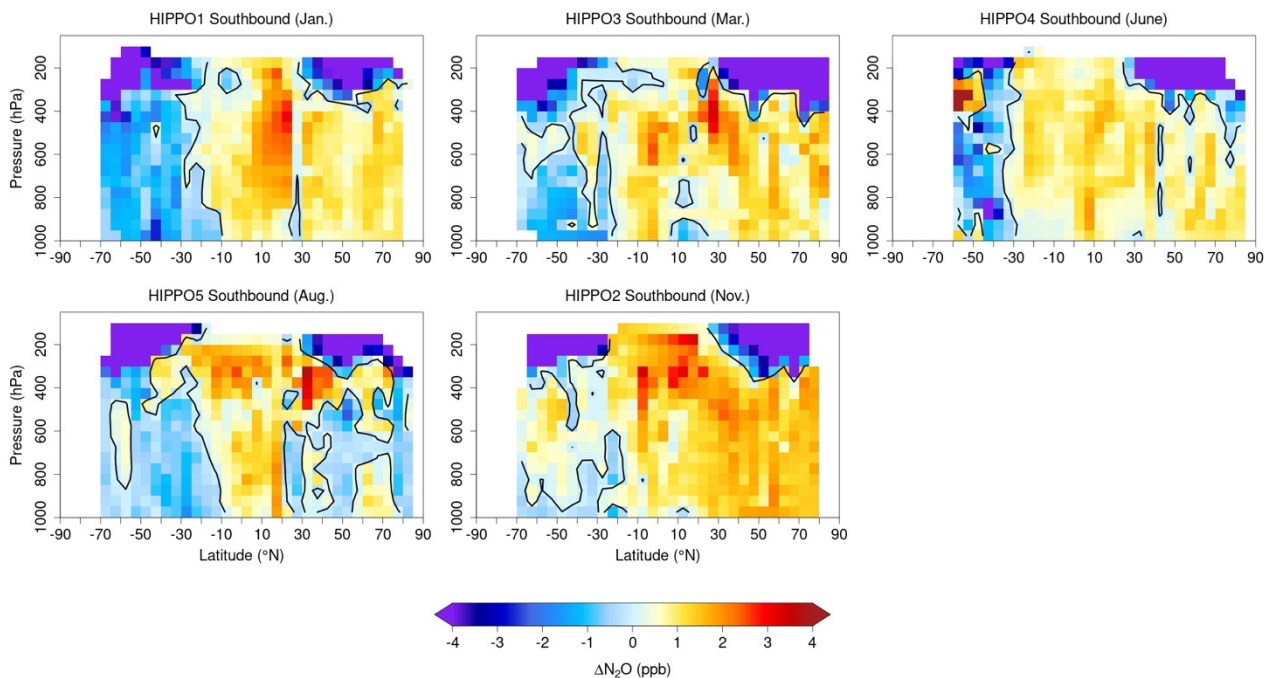


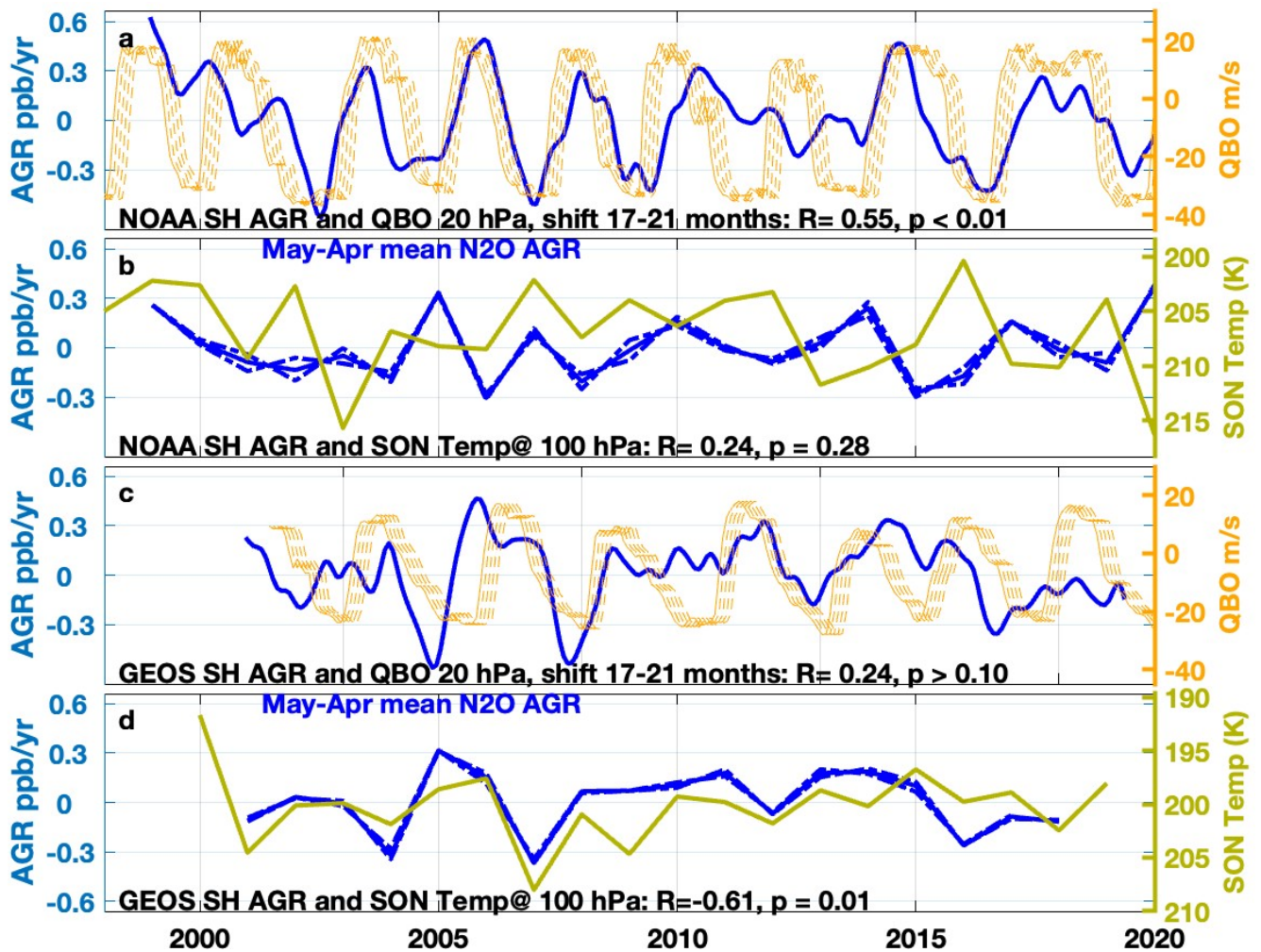
Figure 5: Sequence of five HIPPO pressure-latitude contours of anomalies of N_2O mixing ratio (ppb) arranged to form an annual sequence; from left to right: January, March, June (top row) and August, November (bottom row). Each panel represents a north-to-south transect across latitude with vertical profiling from the surface to 14 km.

3.2 Correlation analysis of the Surface N_2O Atmospheric Growth Rate (AGR)

In this section NOAA surface N_2O AGR anomalies from 1998-2020 are plotted against polar lower stratospheric temperature (PLST) and QBO and ENSO indices, with varying lag times as described in the Methods (Section 2). The analysis focuses on the NOAA global, NH, and SH mean products, with the assumption that a significant correlation between the interannual variability in the N_2O AGR and one or more of the indices can be interpreted to support a causal influence on the N_2O AGR. However, correlation does not prove causation and cannot distinguish possible confounding effects, such as the influence of ENSO on both interhemispheric transport and surface sources. A similar correlation

405 analysis is performed for the GEOSCCM N₂O AGR and the model's internally-generated QBO and PLST fields, with the assumption that similarities between modeled and observed correlations may also support a causal influence.

Figure 6, which presents correlations between the SH surface N₂O AGR and the QBO and PLST indices, first for NOAA observations and next for GEOSCCM output, shows that the QBO is positively correlated to the NOAA N₂O AGR. The optimal correlation ($R = 0.55$, $p < 0.01$) occurs for QBO in the upper stratosphere at 20 hPa with a time shift of about 18 (17-19) months relative to the N₂O time series. In contrast, spring PLST is not significantly correlated to the NOAA surface N₂O AGR in the SH (Fig. 6b). In Fig. 6c, the correlation between GEOSCCM QBO and the SH N₂O AGR is weak ($R =$
415 0.24 , $p > 0.10$) but also positive in sign in the upper stratosphere with an optimal shift in the GEOSCCM QBO of about 19 months, similar to that found for NOAA. In Fig. 6d, GEOSCCM PLST is significantly anticorrelated with the N₂O AGR averaged over a range of different 12-month intervals, with the highest correlation ($R = -0.61$, $p = 0.01$) over the 12-month interval from May-April.



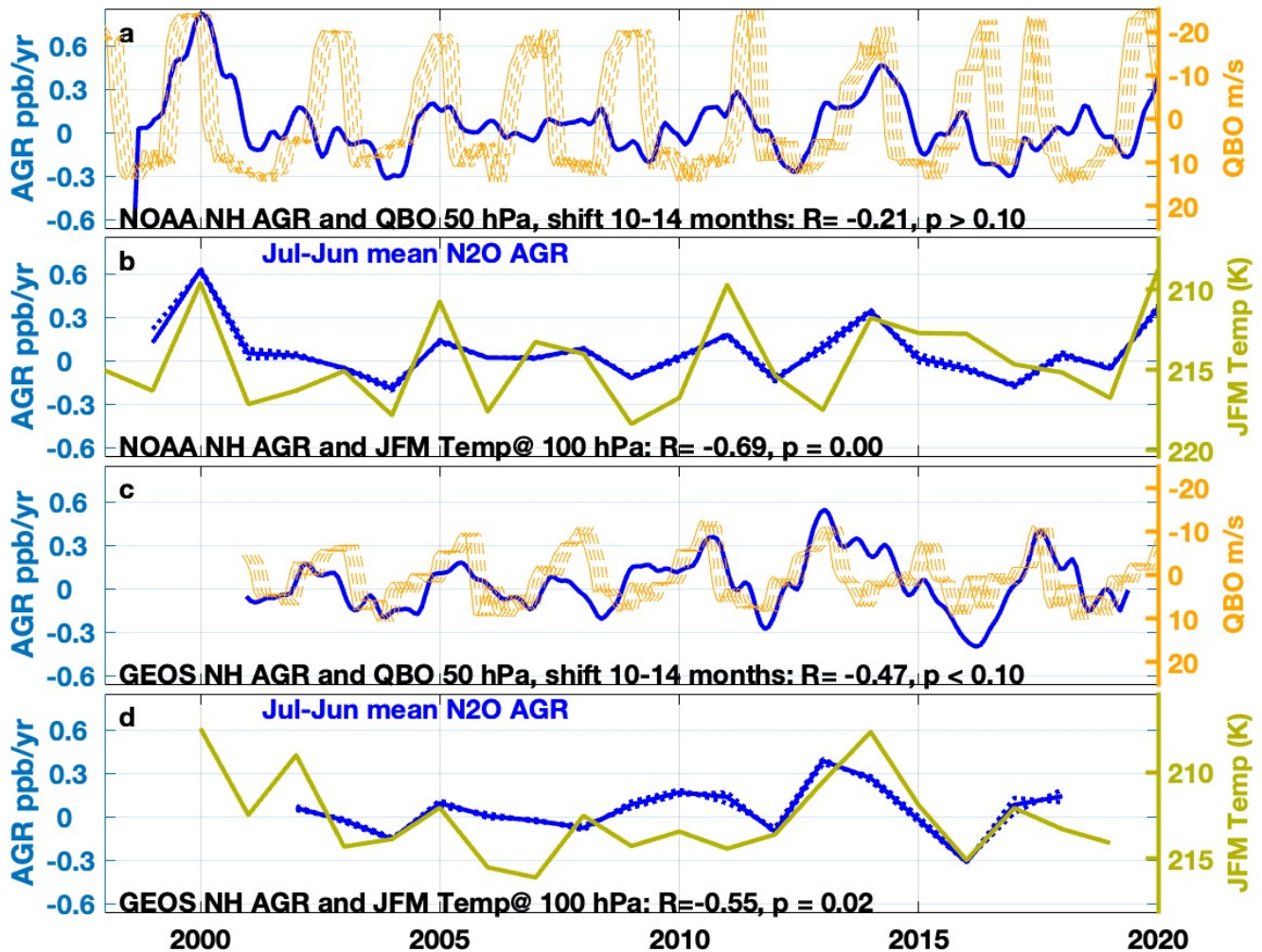
420

425

Figure 6: SH N₂O atmospheric growth rate (AGR in ppb/yr) for (a) NOAA and (c) GEOSCCM plotted with the QBO index at 20 hPa with a 17-21 month forward shift in the index. (b,d) SH N₂O AGR plotted with mean lower stratospheric temperature averaged over 60-90°S for September-November in the year prior to the annual label on the X axis. The AGR is averaged from monthly N₂O data over the ensuing 12 month period May-April (solid blue line), shifted plus or minus 1 month (dotted blue lines), for (b) NOAA and (d) GEOSCCM. Note: to convert to %/yr (AGR units often used in the literature) ppb/yr can be multiplied by 100/323 (~1/3), where 323 is the mean tropospheric mixing ratio of N₂O over 1998-2020.

Figure 7, which presents the corresponding correlations for the NH surface N₂O AGR, shows that, in contrast to the SH, the NOAA NH N₂O AGR is correlated only weakly to the QBO index at all altitudes, and with a negative sign. The highest correlation in the NH occurs for 50 hPa QBO ($R = -0.21$, $p > 0.1$) with a 10-14 months lag (Fig. 7a). However, the NOAA NH N₂O AGR is anticorrelated significantly to winter PLST ($R = -0.69$, $p < 0.001$), with an optimal correlation for the 12-month period from July-June encompassing the January-March PLST average (Fig. 7b). GEOSCCM predicts an

435 anticorrelation ($R = -0.47$, $p < 0.05$) between the QBO and the NH N_2O AGR, which is optimal around 50 hPa with 10-14 month QBO lag, similar to NOAA (Fig. 7c) and also predicts an anticorrelation between PLST and NH N_2O AGR ($R = -0.55$, $p = 0.02$) (Fig. 7d).



440

Figure 7: NH N_2O atmospheric growth rate (AGR in ppb/yr) for (a) NOAA and (c) GEOSCCM plotted with the QBO index at 50 hPa with a 10-14 month forward shift in the index. (b,d) NH N_2O AGR plotted with mean lower stratospheric temperature averaged over 60-90°N for January-March of the year labeled on the X axis. The AGR is averaged from monthly N_2O data over the encompassing 12 month period July-June (solid blue line), shifted plus or minus 1 month (dotted blue lines), for (b) NOAA and (d) GEOSCCM.

445

Figure 8, which presents correlations between the Niño 3.4 index and the NOAA surface N_2O AGR,

shows that that the two are significantly anticorrelated ($R \sim -0.4$, $p < 0.05$) for both the global and SH
 450 N_2O AGR, with little or no monthly lag in the index. In the NH, the anticorrelation is weaker ($R = -$
 0.26 , $p > 0.10$) with an optimal lag of 7 months in the Niño 3.4 index relative to the N_2O AGR (Fig. 8).

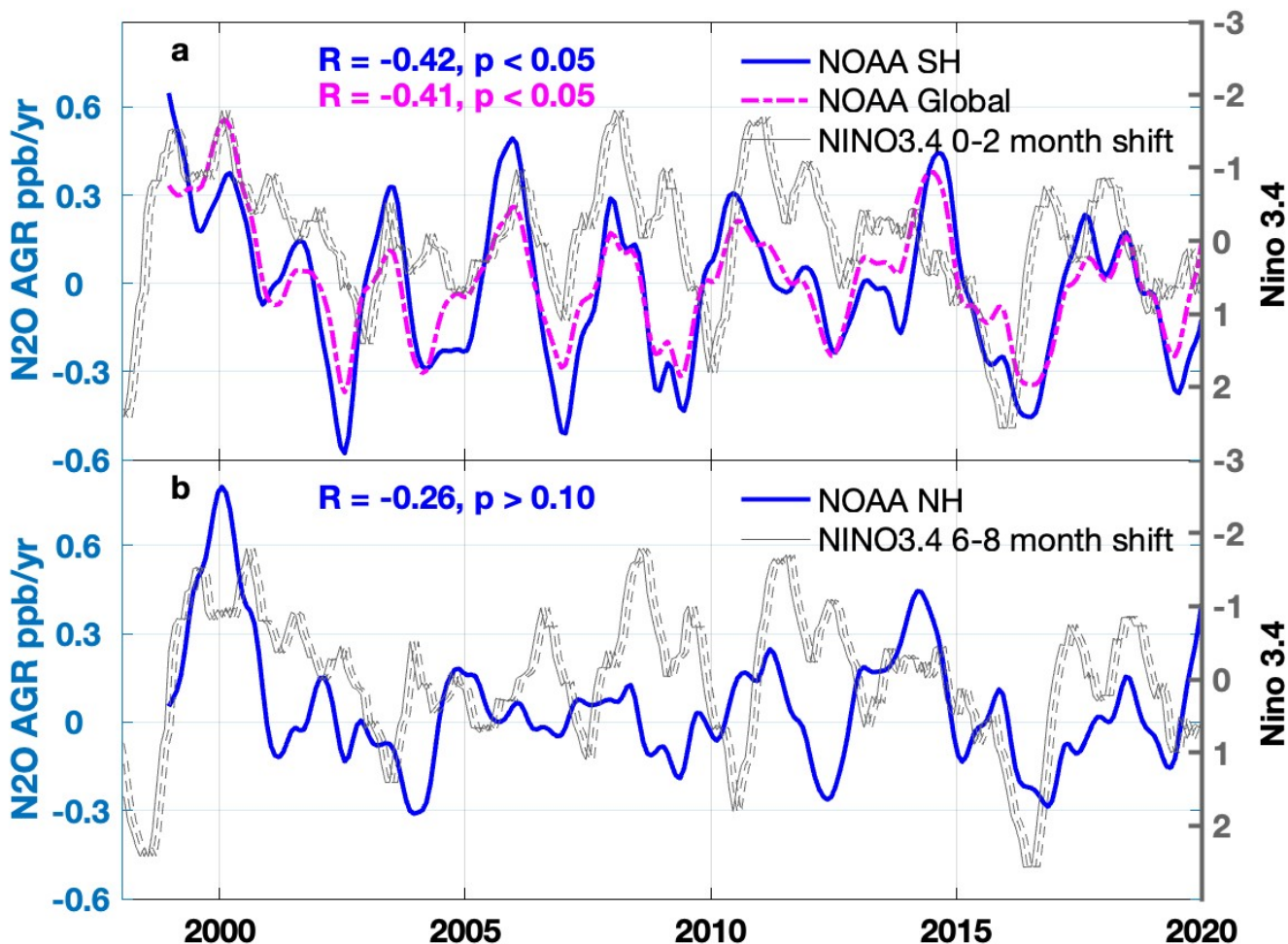


Figure 8: NOAA N_2O atmospheric growth rate (AGR in ppb/yr) plotted with the Niño 3.4 index for a) SH and global mean AGR with a 0-2 month shift in the index and b) NH AGR with a 6-8 month shift in the index.

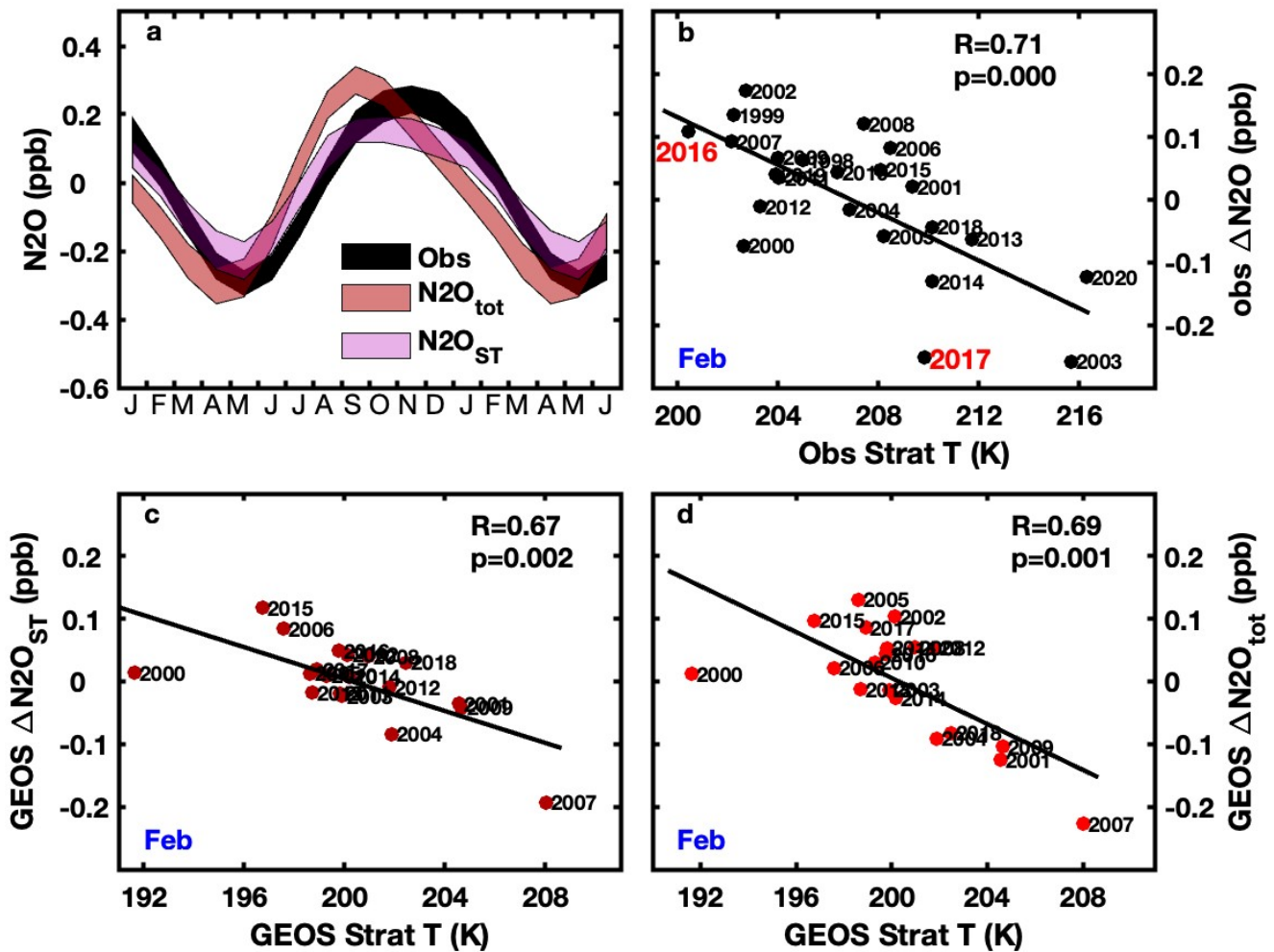
455

3.3 Correlation analysis of N_2O monthly anomalies

The N_2O monthly anomaly correlation analysis is focused solely on PLST, which has one unique value each year that can be plotted against the corresponding N_2O anomaly for any given month. The months selected for this correlation analysis were those surrounding the seasonal N_2O minimum, which is the

460 most distinct feature of the seasonal cycle for NOAA sites at remote mid and high latitudes. These months were hypothesized, based on previous work, as most likely to be influenced by the descent of N₂O-poor air from the stratosphere (*Nevison et al.*, 2011). In contrast, QBO and ENSO are monthly indices for which it is not straightforward to choose a representative month to correlate to the N₂O monthly anomaly, given that the anomaly might result from the cumulative effect over multiple months.

465 Figure 9a shows that the mean seasonal cycles in SH surface N₂O for NOAA and GEOSCCM total N₂O (N₂O_{tot}) and stratospheric N₂O (N₂O_{ST}), as illustrated at South Pole (SPO), all have similar autumn seasonal minimum, within the range of uncertainty as estimated using a bootstrap method. Figure 9b shows that PLST from the previous spring is significantly anticorrelated to NOAA SPO N₂O monthly anomalies in February, when N₂O is descending into its minimum. This correlation is observed in both 470 January and February at SPO as well as several extratropical southern NOAA sites including Cape Grim, Tasmania and Palmer Station, Antarctica. The sign of the correlation is such that more negative surface N₂O anomalies occur during warm years, in which stronger than average descent of N₂O-poor air occurs into the polar lower stratosphere over the austral winter and spring. GEOSCCM simulates 475 similar correlations between PLST and austral summer N₂O anomalies at these sites, both for N₂O_{ST} and N₂O_{tot} in February (Fig. 9c,d), and also March, i.e., the correlations are delayed by about 1 month relative to NOAA surface observations.



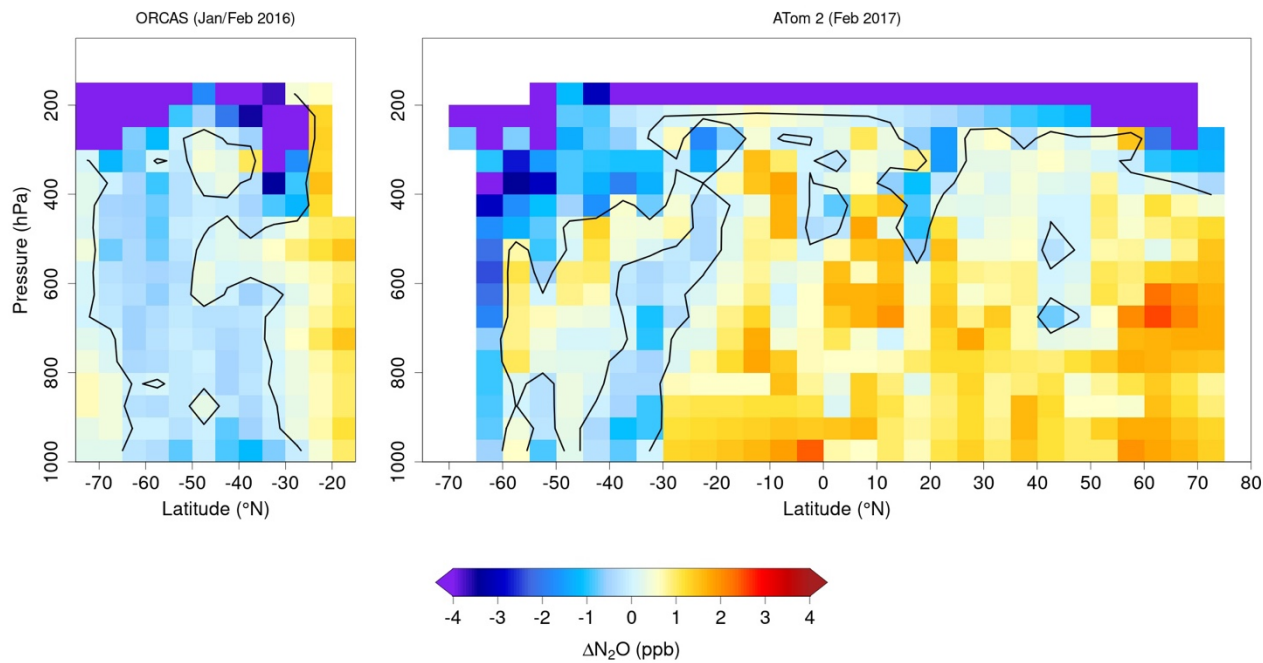
480

Figure 9: Top row shows a) mean seasonal cycles in N_2O for NOAA surface station observations (Obs) and GEOSCCM surface total N_2O (N_2O_{tot}) and stratospheric N_2O (N_2O_{ST}), with uncertainty estimated using a bootstrap method, and b) NOAA surface seasonal anomalies of N_2O mixing ratio (ppb) in February at South Pole spanning 1998-2020, plotted vs. mean lower stratospheric MERRA-2 temperature at 100 hPa averaged over 60-90°S over the previous spring (September-November). The labeled anomalies in 2016 and 2017 correspond to the year of the ORCAS and ATom-2 aircraft surveys, respectively. Bottom row shows GEOSCCM surface seasonal anomalies of N_2O mixing ratio (ppb) for c) N_2O_{ST} and d) N_2O_{tot} in February at South Pole spanning 2000-2019, plotted vs. mean GEOSCCM lower stratospheric temperature, which is sampled the same way as the MERRA-2 temperature.

490

Figure 10, which compares February altitude-latitude N_2O contour plots from the ORCAS and ATom airborne surveys, offers some qualitative support for the observed surface correlations in Fig. 9. The contour plots show more depleted N_2O values in the SH polar upper troposphere during ATom-2, which took place in February 2017 after a relatively warm spring in the Antarctic lower stratosphere (strong BDC), compared to ORCAS, which took place in January-February 2016 after a particularly cold spring

495 (weak BDC). The right panel shows ATom-2 data over the full 65°S to 75°N latitude span, putting the stratospheric influence coming from the southern polar stratosphere into broader perspective. The left panel extends only from 70°S to 20°S because ORCAS was confined to that region. Notably, the positive anomaly in the mid-troposphere observed at 40-60°S during ATom-2, which may be a source plume from the Southern Ocean, tends to contradict the hypothesis that SH tropospheric N₂O was lower
500 overall in 2017 than in 2016.



505 **Figure 10. Anomalies of N₂O in ppb as a function of altitude and latitude from (left panel) ORCAS (Jan.-Feb. 2016) and (right panel) ATom-2 (Jan.-Feb. 2017).**

In contrast to the SH, PLST in the NH from the previous winter is not correlated significantly to N₂O monthly anomalies at extratropical surface sites for either NOAA or GEOSCCM in any of the months surrounding the NH N₂O seasonal minimum, with the exception of Mace Head, Ireland, where a
510 negative correlation is found in July in GEOSCCM (Supplementary Fig. S3).

4. Discussion

The atmospheric N₂O observations and model results assembled here present several new lines of
515 evidence that the stratosphere helps drive the seasonal minimum in tropospheric N₂O and also
influences its atmospheric growth rate. First, the vertical cross sections of atmospheric N₂O from
aircraft provide a broad-scale perspective, in which N₂O-poor air enters the winter polar lower
stratosphere, crosses the tropopause around the time of polar vortex breakup, and descends downward
and equatorward, reaching Earth's surface by summer or early fall. These patterns are seen in both the
520 NOAA empirical background and in global airborne survey data (Fig. 3, 4, 5). Second, GEOSCCM
simulations show similar 3-dimensional patterns to those in the NOAA empirical background (Fig. 3)
and also yield correlations between the surface N₂O AGR with internally modeled QBO and PLST
indices that are similar to those found in observations (Fig. 6, 7). In addition, GEOSCCM predicts
correlations between February surface N₂O anomalies and PLST in the SH, both for total N₂O, similar
525 to those observed, and for the tagged stratospheric tracer N₂O_{ST} (Fig. 9).

The comparison of GEOSCCM output to NOAA observations, while qualitatively supporting a
stratospheric influence on the troposphere, also raises questions. The phasing of the GEOSCCM N₂O
seasonal cycle is delayed relative to observations, especially in the NH, and the model simulates a too-
530 long delay in propagating stratospheric signals down to the surface (Fig. 1,3). Diabatic descent in the
stratosphere has been shown to be underestimated in atmospheric models (e.g. *Brühl et al.*, 2007;
Khosrawi et al., 2009; 2018) and this may also be the case for air crossing into the troposphere.
Another issue is that the seasonality of surface N₂O emissions may not be well represented in the
GEOSCCM simulation, e.g., summer soil emissions are from a soil biogeochemistry model and may be
535 overestimated, leading to unrealistic surface maxima in July (*Saikawa et al.*, 2013; *Nevison et al.*, 2018;
Liang et al., 2022).

With respect to the aircraft data, the NOAA empirical background and QLCS vertical cross sections,
while showing similar features, are not matched exactly for comparison. QCLS data are measured

540 across a narrow longitude band of the flight track for any given latitude on a limited number of days,
while the NOAA empirical background is shown as a monthly mean, zonally averaged across most of
the western hemisphere (170°-50°W). Consequently, QCLS data are more likely to display synoptic-
scale variability, such as the apparent surface source plume over the Southern Ocean seen in Fig. 10.

4.1 Correlation to stratospheric indices: signs and magnitudes

545 The results of the correlation analysis based on NOAA surface N₂O data are similar to those found in
previous studies based on Advanced Global Atmospheric Gases Experiment (AGAGE) surface N₂O
data (Prinn *et al.*, 2000; Nevison *et al.*, 2007; 2011). In general, these correlations are weak, in part
because the variability in surface N₂O is very small compared to its mean tropospheric mixing ratio.
Nevertheless, PLST in the NH correlates significantly to NOAA surface N₂O AGR anomalies (Fig. 7b)
550 and PLST in the SH correlates significantly to monthly N₂O anomalies in February near the time of the
seasonal N₂O minimum (Fig. 9b). The negative sign of these correlations is easily understood and
consistent with more downward transport of N₂O-poor air and warming of the polar lower stratosphere
in years with stronger BDC, with subsequent cross-tropopause transport that deepens the descent of
tropospheric N₂O into its seasonal minimum and slows the observed AGR of surface N₂O.

555

The reason for the positive correlation of the QBO index with the SH surface N₂O AGR (Fig. 6a,c) is
less obvious. A similar correlation in the SH, but not the NH, has been observed in other studies but not
fully explained (Ray *et al.*, 2020). In our analysis, the positive correlation between the QBO and the SH
N₂O AGR is strongest for the QBO at 20 hPa with 18 months lag and then weakens with decreasing
560 QBO altitude down to 100 hPa, with a concurrent decrease in the optimal lag, likely due to the time
needed for downward propagation of QBO winds (Supplementary Fig. S4). At 50 hPa, we find an
optimal lag time of 10-12 months (R = 0.39), consistent with Ray *et al.* (2020) (who only presented
results for QBO = 50 hPa).

565 Photochemical destruction of N₂O is highest when QBO winds above 30 hPa are in the westerly
(positive) phase and lower altitude QBO winds are in the easterly (negative) phase. This configuration

is associated with increased vertical upwelling in the tropical lower stratosphere, which transports more N₂O to its peak loss region around 32 km (*Strahan et al.*, 2021; *Ruiz et al.*, 2021). Thus the magnitude of QBO-associated photochemical destruction per se cannot be the main driver of the stratospheric influence on surface N₂O, since one would logically expect a negative correlation (i.e., slower growth in the troposphere due to more stratospheric N₂O loss during positive QBO). *Ruiz et al.* (2021) similarly concluded that surface variability in N₂O is not correlated directly to the QBO-driven variability in stratospheric loss, but rather by dynamical variations in cross tropopause fluxes of air, which are governed at least in part by the BDC.

575

The dynamics of the QBO, its interaction with the BDC and ultimate influence on surface N₂O are complex. However, the positive correlation of QBO, peaking at 20 hPa, with the SH N₂O AGR, could be explained in the context of *Strahan et al.* (2015), as described in detail in the Supplementary Materials, Section S2. Briefly, the QBO has an associated meridional circulation, which transports N₂O-poor air poleward from the region of peak photochemical destruction in the tropics between about 30 hPa to 10 hPa in altitude. Paradoxically, this meridional circulation transports less N₂O-poor air toward the poles during the phase when the QBO is positive above 30 hPa (i.e., when photochemical destruction is highest). The N₂O-poor air subsequently is trapped in the Antarctic polar vortex and undergoes BDC-driven diabatic descent, in isolation from mixing with lower latitudes, arriving largely intact in the lower stratosphere and eventually at earth's surface, with a long lag time consistent with the 18 month lag found in Fig. 6a.

In the NH, the planetary wave activity that drives the BDC is stronger due to the more variable topography and stronger land-sea contrasts. Consequently, the BDC-driven descent into the winter pole is more strongly seasonal and the NH polar vortex is less isolated (*Holton et al.*, 1995; *Scaife and James*, 2000, *Butchart*, 2014, *Kidston et al.*, 2015), such that any signal associated with the QBO meridional circulation does not transport intact to lower altitudes (*Strahan et al.*, 2015). This may

590

explain why, for both NOAA surface stations and GEOSCCM, the NH N₂O AGR is more strongly correlated to PLST (a proxy for the BDC) than it is to the QBO, consistent with *Ruiz et al. (2021)*.

595

In contrast to the NH, the NOAA SH surface N₂O AGR does not correlate to PLST. This result is somewhat puzzling given the significant correlation between PLST and NOAA N₂O February anomalies at SH high latitude surface sites (Fig. 9). It appears that the impact of the stratosphere in austral summer as tropospheric N₂O descends into its seasonal minimum is not sufficient to influence the N₂O AGR across the whole SH over the entire year. The SH N₂O AGR results may reflect the strong preservation of the QBO signal that is ultimately transported into the troposphere, as discussed above, combined with the relatively weaker BDC in the SH and/or the interference of ENSO-driven signals discussed below.

600

610

4.2 Correlations with ENSO

The NOAA surface station N₂O AGR correlation with the ENSO index is significant in the SH ($R = -0.42$, $p < 0.05$, 0-2 month phase shift) but weaker in the NH ($R = -0.26$, $p > 0.10$, 7 month optimal phase shift) (Fig. 10). The correlation in the SH could in part reflect meteorological shifts in the tropical low level convergence pattern during positive (El Niño) conditions. For atmospheric gases with a positive north-south latitudinal gradient, these shifts result in a lessened influence of winds from the NH on the tropical SH and an increased influence of southeasterly winds. The NOAA Samoa site at 14°S, which strongly influences the cosine-latitude-weighted SH average, is known to be affected by these kinds of wind shifts (*Prinn et al., 1992; Nevison et al., 2007*). The fact that the N₂O AGR correlation with ENSO is considerably weaker in the NH than in the SH suggests a limited impact of ENSO on NH N₂O and supports the hypothesis that reduced north-to-south transport during positive ENSO contributes to the correlation observed in the SH.

610

615

The negative correlation between N₂O AGR and ENSO also may reflect a true reduction in the biogeochemical N₂O source during the positive ENSO phase, for example, due to drought over tropical land or due to reduced upwelling in the tropical ocean (*Ishijima et al., 2009; Thompson et al., 2013*).

620 The most well documented biogeochemical response of N₂O to ENSO events occurs in the Eastern Tropical South Pacific (ETSP), a well known oxygen minimum zone (OMZ) and hot spot of oceanic N₂O emissions (Arévalo-Martínez, 2015; Ji *et al.*, 2019). El Niño conditions decrease upwelling in the ETSP, thereby reducing the surface productivity, deepening the oxycline, contracting the OMZ and decreasing the N₂O sea-to-air flux (Ji *et al.*, 2019; Babbín *et al.*, 2015).

625

However, less than one quarter of the total N₂O budget likely comes from oceanic emissions, of which the ETSP is only one component (Yang *et al.*, 2020; Canadell *et al.*, 2021). This raises questions about whether a reduced ETSP source (or a strengthened source during La Niña periods) has enough leverage to control the overall N₂O AGR. Ruiz *et al.* (2021) removed the stratospheric influence from surface
630 N₂O data to infer a source of ~ 1 Tg N (about 5% of the total annual N₂O source) associated with the 2010 La Niña event, which could have come from tropical land or ocean, or some combination of both. Similarly, Kort *et al.* (2011) found evidence of strong episodic pulses of ~ 1 Tg N from tropical regions, based on maxima in QCLS N₂O data measured in the middle and upper troposphere during aircraft campaigns in 2009. These pulses were not tied specifically to an ENSO event but rather more generally
635 demonstrated the strength of the tropical N₂O source.

5. Summary and Outlook

GEOSCCM simulations with a tagged stratospheric tracer show that N₂O-poor air descends throughout the winter into the polar lower stratosphere, crosses the tropopause in spring or early summer, and descends downward and equatorward, transmitting a diluted but still coherent signal to Earth's surface
640 in late summer to early autumn (August-September in the NH, April-May in the SH). The GEOSCCM simulations are corroborated by N₂O observations from aircraft, which provide direct evidence for a stratospheric influence on tropospheric N₂O that previously was inferred primarily based on correlations of surface N₂O data to stratospheric indices. In support of the model and aircraft results, and consistent with previous studies, significant correlations are found between the N₂O AGR observed at long-term
645 NOAA surface monitoring sites and either the QBO index in the SH or PLST in the NH, where PLST is a proxy for the strength of the BDC. Correlations between the N₂O AGR and ENSO indices are also

statistically significant in the SH, suggesting a joint influence of ENSO and the stratosphere on the AGR in that hemisphere. The QBO influences the rate at which N₂O is transported to and destroyed in the tropical stratosphere, but complex atmospheric dynamics buffer how variations in the N₂O photochemical loss rate are transmitted across the tropopause to modulate the surface N₂O AGR. Cross-tropopause transport at high latitudes is linked closely to the BDC and appears to be a more direct influence than the QBO on the N₂O AGR in the NH. In the SH in contrast, the combination of a better-preserved QBO signal and weaker BDC may lead to a direct (albeit with a ~18 month lag) correlation between the QBO and the SH N₂O surface AGR, consistent with current knowledge of stratospheric dynamics.

The solar cycle is an additional influence on variability in N₂O that may be worth investigating in future work. While previous studies have estimated a relatively small effect over the 2000s and 2010s due to low solar activity (Ruiz et al., 2021; Prather et al., 2023), solar cycle-driven changes in the UV flux affect N₂O photolysis both directly and indirectly through the impact stratospheric O₃. Another important issue is the impact on N₂O of climate change driven increases in the strength of the BDC (Garny et al., 2013; Butchart et al., 2014; Fu et al., 2019). Of particular relevance to the results presented here are studies based on ground or satellite based N₂O observations that find a decrease in the N₂O lifetime (Prather et al., 2023) and interhemispheric differences in stratospheric N₂O trends (Minganti et al., 2022). Finally, to help refine our understanding of variability in tropospheric N₂O, long-term monitoring at surface and aircraft-based sites is essential and would be complemented by more global airborne surveys extending into the lower stratosphere. The latter provide new insights into stratospheric influences on tropospheric N₂O and advance our ability to interpret and quantify surface N₂O sources.

670 **Code Availability**

Codes are available from the corresponding author upon request.

Data Availability

NOAA N₂O data can be obtained by contacting xin.lan@noaa.gov or through the NOAA Global Monitoring Laboratory at https://gml.noaa.gov/aftp/data/trace_gases/n2o/flask/. QCLS N₂O data are
675 openly available and archived in the Oak Ridge National Laboratory Distributed Active Archive Center (ORNL DAAC) <https://doi.org/10.3334/ORNLDAAC/1925> (ATom), and at the National Center for Atmospheric Research (NCAR) <https://doi.org/10.5065/D6SB445X> (ORCAS) and https://doi.org/10.3334/CDIAC/HIPPO_010 (HIPPO).

Author contributions

680 CDN designed and carried out the analysis and prepared the main manuscript and most of the figures. QL implemented separate stratospheric and tropospheric N₂O tracers in GEOSCCM and provided model output. PN computed QBO indices and MERRA stratospheric temperatures and provided guidance on stratospheric dynamics. BBS, RC, YG and EK provided QCLS N₂O data and BBS created contour plots of the QCLS data. XL and GD provided N₂O surface data. All authors reviewed and
685 approved the manuscript.

Competing Interests

The authors declare they have no conflicts of interest.

Acknowledgments

690 CDN and QL acknowledge support from the NASA MAPS program (award 16-MAP16-0049). The authors are grateful to Arlyn Andrews, Colm Sweeney, Bradley Hall, Ed Dlugokencky, Steve Wofsy, Bruce Daube, and many others who have made this study possible, through collection and analysis of surface station and NOAA aircraft flasks, in situ NOAA station measurements, and QCLS aircraft campaign observations. The HIPPO and ORCAS observations, and the contributions of BBS were supported by the National Center for Atmospheric Research, which is a major facility sponsored by the
695 National Science Foundation under Cooperative Agreement No. 1852977. The authors thank Dr. Farahnaz Khosrawi and 2 other anonymous reviewers whose detailed and helpful comments much improved the manuscript.

References

- 700 Akima, H.: A Method of Bivariate Interpolation and Smooth Surface Fitting for Irregularly Distributed Data Points, ACM Transactions on Mathematical Software, Vol. 4, No. 2, June 1978, pp. 148-159. Copyright 1978, Association for Computing Machinery, Inc, 1978
- Arévalo-Martínez, D. L., Kock, A., Löscher, C. R., Schmitz, R. A. & Bange, H. W.: Massive nitrous oxide emissions from the tropical South Pacific Ocean, Nat. Geosci., 8, 530, 2015.
- 705 Babbin, A.R., Bianchi, D., Jayakumar, A, and Ward, B. B.: Rapid nitrous oxide cycling in the suboxic ocean, Science, 348, doi:10.1126/science.aaa8380, 2015.

- Baldwin, M.P., Gray, L.J., Dunkerton, T.J., Hamilton, K., Haynes, P.H., Randel, W.J., Holton, J.R., Alexander, M.J., Hirota, I., Horinouchi, T., Jones, D.B.A., Kinnersley, J.S., Marquardt, C., Sato, K., Takahashi, M.: The quasi-biennial oscillation, *Reviews of Geophysics*, 39(2), 179-229, 2001.
- 710 Bouwman, A.F. and Taylor, J.A.: Testing high-resolution nitrous oxide emission estimates against observations using an atmospheric transport model, *Global Biogeochem. Cy.*, 10, 307-318, 1996.
- Bouwman, A.F., van der Hoek, K.W., and Olivier, J.G.J.: Uncertainties in the global source distribution of nitrous oxide, *J. Geophys. Res.*, 100, 2785-2800, 1995.
- 715 Brühl, C., Steil, B., Stiller, G., Funke, B., and Jöckel, P.: Nitrogen compounds and ozone in the stratosphere: comparison of MIPAS satellite data with the chemistry climate model ECHAM5/MESSy1, *Atmos. Chem. Phys.*, 7, 5585–5598, <https://doi.org/10.5194/acp-7-5585-2007>, 2007.
- Butchart, N.: *Reviews of Geophysics The Brewer-Dobson Circulation*, *Rev. Geophys*, 52, 157–184. <https://doi.org/10.1002/2013RG000448>, 2014.
- 720 Canadell, J. G., P. M. S. Monteiro, M. H. Costa, L. Cotrim da Cunha, P. M. Cox, A. V. Eliseev, S. Henson, M. Ishii, S. Jaccard, C. Koven, A. Lohila, P. K. Patra, S. Piao, J. Rogelj, S. Syampungani, S. Zaehle, K. Zickfeld: Global Carbon and other Biogeochemical Cycles and Feedbacks. In: *Climate Change 2021: The Physical Science Basis. Contribution of Working Group I to the Sixth Assessment Report of the Intergovernmental Panel on Climate Change* (Masson-Delmotte, V., P. Zhai, A. Pirani, S. L. Connors, C. Péan, S. Berger, N. Caud, Y. Chen, L. Goldfarb, M. I. Gomis, M. Huang, K. Leitzell, E. Lonnoy, J.B.R. Matthews, T. K. Maycock, T. Waterfield, O. Yelekçi, R. Yu and B. Zhou (eds.)). Cambridge University Press, 2021.
- 725 Earth Systems Research Laboratory, Multivariate ENSO Index (MEI). NOAA (2017).
- 730 Elkins, J.W, and Dutton, G.S.: Nitrous oxide and sulfur hexafluoride (in 'State of the Climate in 2008'), *Bull. Amer. Meteor. Soc*, 90, S38-S39, 2009.
- Forster, P., Ramaswamy, V., Artaxo, P., Berntsen, T., Betts, R., Fahey, D.W., Haywood, J., Lean, J., Lowe, D.C., Myhre, G., Nganga, J., Prinn, R., Raga, G., Schulz, M. and Van Dorland, R.: Changes in Atmospheric Constituents and in Radiative Forcing. In: *Climate Change 2007: The Physical Science Basis. Contribution of Working Group I to the Fourth Assessment Report of the Intergovernmental Panel on Climate Change*. Cambridge University Press Cambridge, United Kingdom and New York, NY, USA, 2007.
- 735 Fu Q., Solomon S., Pahlavan H.A., Lin P.: Observed changes in Brewer-Dobson circulation for 1980-2018, *Environmental Research Letters*, 14 (11), 114026, DOI: 10.1088/1748- 9326/ab4de7, 2019.
- 740 Garny H., Bodeker G.E., Smale D., Dameris M., Grewe V.: Drivers of hemispheric differences in return dates of mid-latitude stratospheric ozone to historical levels, *Atmospheric Chemistry and Physics*, 13 (15),7279 - 7300, DOI: 10.5194/acp-13-7279-2013, 2013.
- 745 Gonzalez, Y., Commane, R., Manninen, E., Daube, B.C., Schiferl, L., McManus, J.B., McKain, K, Hints, E.J., Elkins, J.W., Montzka, S.A.: Impact of stratospheric air and surface emissions on tropospheric nitrous oxide during ATom, *Atmospheric Chemistry and Physics Discussions*, <https://doi.org/10.5194/acp-2021-167>, 2021.

- 750 Gurney, K. R., Law, R.M., Denning, A.S., Rayner, P.J., Pak, B.C., Baker, D.F., Bousquet, P.,
Bruhwiler, L., Chen, Y.-H., Ciais, P., Fung, I.Y., Heimann, M., John, J., Maki, T., Maksyutov,
S., Peylin, P., Prather, M., Taguchi, S.: Transcom 3 inversion intercomparison: Model mean
results for the estimation of seasonal carbon sources and sinks, *Global Biogeochem. Cycles*, 18,
GB1010, doi:10.1029/2003GB002111, 2004.
- Hall, B. D., Dutton, G.S., and Elkins, J. W.: The NOAA nitrous oxide standard scale for atmospheric
observations, *J. Geophys. Res.*, 112, D09305, doi:10.1029/2006JD007954, 2007.
- 755 Hall, B. D., Dutton, G. S., Mondeel, D. J., Nance, J. D., Rigby, M., Butler, J. H., Moore, F. L., Hurst, D.
F. and Elkins, J. W.: Improving measurements of SF₆ for the study of atmospheric transport and
emissions, *Atmos. Meas. Tech.*, 4, 2441-2451, doi: 10.5194/amt-4-2441-2011, 2011.
- Hammerling, D. M., Michalak, A. M., Kawa, S. R.: Mapping of CO₂ at High Spatiotemporal Resolution
using Satellite Observations: Global Distributions from OCO-2, *Journal of Geophysical*
760 *Research*, 117, D06306, doi:10.1029/2011JD017015, 2012.
- Hirsch, A.I., Michalak, A.M., Bruhwiler, L.M., Peters, W., Dlugokencky, E.J. and Tans, P.P.: Inverse
modeling estimates of the global nitrous oxide surface flux from 1998-2001, *Global*
Biogeochem. Cy., 20, GB1008, doi:10.1029/2004GB002443, 2006.
- 765 Holton, J.R., Haynes, P.H., McIntyre, M.E., Douglass, A.R., Rood, R.B. and Pfister, L.: Stratosphere-
troposphere exchange, *Rev. Geophys.*, 33(4), 403-439, 1995.
- Holton, J.: An Introduction to Dynamic Meteorology, no. v. 1 in *An Introduction to Dynamic*
Meteorology, Elsevier Science, available at: <https://books.google.be/books?id=fhW5oDv3EPsC>,
2004.
- 770 Huang, J., Golombek, A., Prinn, R., Weiss, R., Fraser, P., Simmonds, P., Dlugokencky, E.J., Hall, B.,
Elkins, J., Steele, P., Langenfelds, R., Krummel, P., Dutton, G., and Porter, L.: Estimation of
regional emissions of nitrous oxide from 1997 to 2005 using multinet network measurements, a
chemical transport model, and an inverse method, *J. Geophys. Res.*, 113, D17313,
doi:10.1029/2007JD009381, 2008.
- 775 Ishijima, K., Patra, P.K., Takigawa, M., Machida, T., Matsueda, H., Sawa, Y., Steele, L.P., Krummel,
P.B., Langenfelds, R.L., Aoki, S. and Nakazawa, T.: The stratospheric influence on the seasonal
cycle of nitrous oxide in the troposphere as deduced from aircraft observations and model
simulations, *J. Geophys. Res.*, 115, D20308, doi:10.1029/2009JD013322, 2010.
- 780 Ji, Q., Babbin, A.R., Jayakumar, A., Oleynik, S. and Ward, B.B.: Nitrous oxide production by
nitrification and denitrification in the Eastern Tropical South Pacific oxygen minimum zone,
Geophys. Res. Lett., 42(24), 10,755–10,764, doi:10.1002/2015gl066853, 2015.
- Ji, Q. et al.: Investigating the effect of El Niño on nitrous oxide distribution in the eastern tropical South
Pacific. *Biogeosciences*, 16(9), 2079–2093, doi:10.5194/bg-16-2079-2019, 2019.
- Jiang, X, Ku, W.L., Shia, R.-L., Li, Q., Elkins, J.W., Prinn, R.G., Yung, Y.L.: Seasonal cycle of N₂O:
Analysis of data, *Global Biogeochem. Cy.*, 21, GB1006, doi:10.1029/2006GB002691, 2007.
- 785 Jin, X. and Gruber, N.: Offsetting the radiative benefit of ocean iron fertilization by enhancing N₂O
emissions, *Geophys. Res. Lett.* 30(24), 2249, 2003.
- Jin, X., Najjar, R.G., Louanchi, F., and Doney, S.C.: A modeling study of the seasonal oxygen budget
of the global ocean, *J. Geophys. Res.*, 112, C05017, doi:10.1029/2006JC003731, 2007.

- 790 Kalnay, E., Kanamitsu, M., Kistler, R., Collins, W., Deaven, D., Gandin, L., Iredell, M., Saha, S.,
White, G., Woollen, J., Zhu, Y., Leetmaa, A., Reynolds, R., Chelliah, M., Ebisuzaki, W.,
Higgins, W., Janowiak, J., Mo, K.C., Ropelewski, C., Wang, J., Jenne, R., Joseph, D.: The
NMC/NCAR 40-year reanalysis project, *B. Am. Meteorol. Soc.*, 77, 437– 471, 1996.
- 795 Khosrawi, F., Müller, R., Proffitt, M. H., Ruhnke, R., Kirner, O., Jöckel, P., Grooß, J.-U., Urban, J.,
Murtagh, D., and Nakajima, H.: Evaluation of CLaMS, KASIMA and ECHAM5/MESSy1
simulations in the lower stratosphere using observations of Odin/SMR and ILAS/ILAS-II,
Atmos. Chem. Phys., 9, 5759– 5783, <https://doi.org/10.5194/acp-9-5759-2009>, 2009.
- 800 Khosrawi, F., Kirner, O., Stiller, G., Höpfner, M., Santee, M. L., Kellmann, S., and Braesicke, P.:
Comparison of ECHAM5/MESSy Atmospheric Chemistry (EMAC) simulations of the Arctic
winter 2009/2010 and 2010/2011 with Envisat/MIPAS and Aura/MLS observations, *Atmos.*
Chem. Phys., 18, 8873–8892, <https://doi.org/10.5194/acp-18-8873-2018>, 2018.
- Kidston, J., Scaife, A., Hardiman, S. et al.: Stratospheric influence on tropospheric jet streams, storm
tracks and surface weather, *Nature Geosci* 8, 433–440, <https://doi.org/10.1038/ngeo2424>, 2015.
- 805 Kort, E. A., Patra, P. K., Ishijima, K., Daube, B. C., Jiménez, R., Elkins, J.W., Hurst, D., Moore, F. L.,
Sweeney, C. and Wofsy, S. C.: Tropospheric distribution and variability of N₂O: Evidence for
strong tropical emissions, *Geophys. Res. Lett.*, 38, L15806, doi:10.1029/2011GL047612, 2011.
- Kroeze, C., Mosier, A. and Bouwman, L.: Closing the global N₂O budget: A retrospective analysis
1500-1994, *Global Biogeochemical Cycles*, 13, 1-8, 1999.
- 810 Lambert, A., Read, W. G., Livesey, N. J., Santee, M.L., Manney, G.L., Froidevaux, L., Wu, D.L.,
Schwartz, M.J., Pumphrey, H.C., Jimenez, C., Nedoluha, G.E., Cofield, R.E., Cuddy, D.T.,
Daffer, W.H., Drouin, B.J., Fuller, R.A., Jarnot, R.F., Knosp, B.W., Pickett, H.M., Perun, V.S.,
Snyder, W.V., Stek, P.C., Thurstans, R.P., Wagner, P.A., Waters, J.W., Jucks, K.W., Toon,
G.C., Stachnik, R.A., Bernath, P.F., Boone, C.D., Walker, K.A., Urban, J., Murtagh, D., Elkins,
J.W., Atlas, E.: Validation of the Aura Microwave LihPa Sounder middle atmosphere water
vapor and nitrous oxide measurements, *J. Geophys. Res.*, 112, D24S36,
815 doi:10.1029/2007JD008724, 2007.
- Lan, X., Dlugokencky, E.J., Mund, J.W., Crotwell, A.M., Crotwell, M.J., Moglia, E., Madronich, M.,
Neff, D. and Thoning, K.W.: Atmospheric Nitrous Oxide Dry Air Mole Fractions from the
NOAA GML Carbon Cycle Cooperative Global Air Sampling Network, 1997-2021, Version:
2022-11-21, <https://doi.org/10.15138/53g1-x417>, 2022.
- 820 Lan, X., Tans, P., Thoning, K.: NOAA Global Monitoring Laboratory: NOAA Greenhouse Gas Marine
Boundary Layer Reference - N₂O. (Data set). NOAA GML. [https://doi.org/10.15138/83W5-
DK71](https://doi.org/10.15138/83W5-DK71), 2023.
- 825 Liang, Q., Stolarski, R.S., Douglass, A.R., Newman, P.A. and Nielsen, J.E.: Evaluation of emissions
and transport of CFCs using surface observations and their seasonal cycles and the GEOS CCM
simulation with emissions-based forcing, *J. Geophys. Res.*, 113, D14302,
doi:10.1029/2007JD009617, 2008.
- Liang, Q., Douglass, A.R., Duncan, B.N., Stolarski, R.S. and Witte, J.C.: The governing processes and
timescales of stratosphere-to-troposphere transport and its contribution to ozone in the Arctic
troposphere, *Atmos. Chem. Phys.*, 9, 3011-3025, 2009.

- 830 Liang, Q., Nevison, C., Dlugokencky, E., Hall, B. D., & Dutton, G.: 3-D atmospheric modeling of the global budget of N₂O and its isotopologues for 1980–2019: The impact of anthropogenic emissions. *Global Biogeochemical Cycles*, 36, e2021GB007202. <https://doi.org/10.1029/2021GB007202>, 2022.
- Lickley, M., Solomon, S., Kinnison, D., Krummel, P., Mühle, J., O’Doherty, S., et al.: Quantifying the imprints of stratospheric contributions to interhemispheric differences in tropospheric CFC-11, CFC-12, and N₂O abundances. *Geophys. Res. Lett.*, 48, e2021GL093700. <https://doi.org/10.1029/2021GL093700>, 2021.
- 835 Lovenduski, N.S., Gruber, N., Doney, S.C., and Lima, I.D.: Enhanced CO₂ outgassing in the Southern Ocean from a positive phase of the Southern Annular Mode, *Glob. Biogeochem. Cycles*, 21, GB2026, doi:10.1029/2006GB002900, 2007.
- 840 Lueker, T.J., Walker, S.J., Vollmer, M.K., Keeling, R.F., Nevison, C.D. and Weiss, R.F.: Coastal upwelling air-sea fluxes revealed in atmospheric observations of O₂/N₂, CO₂ and N₂O, *Geophys. Res. Lett.*, 30, 1292, 2003.
- MacFarling Meure, C., Etheridge, D. M., Trudinger, C. M., Steele, L. P., Langenfelds, R. L., van 845 Ommen, T., Smith, A. and Elkins, J. W.: Law Dome CO₂, CH₄, and N₂O ice core records extended to 2000 years BP, *Geophys. Res. Lett.*, 33, L14810, doi:10.1029/2006GL026152, 2006.
- Mahowald, N. M., Rasch, P. J., Eaton, B. E., Whittlestone, S. and Prinn, R. G.: Transport of radon-222 850 to the remote troposphere using the Model of Atmospheric Transport and Chemistry and assimilated winds from ECMWF and the National Center for Environmental Prediction/NCAR, *J. Geophys. Res.*, 102, 28139–28151, 1997.
- Masarie, K. A. and Tans, P.P.: Extension and integration of atmospheric carbon dioxide data into a globally consistent measurement record, *Journal of Geophysical Research-Atmospheres*, 100, D6, 11593-11610, 1995.
- 855 McPhaden, M. J., et al.: The tropical ocean-global atmosphere observing system: A decade of progress, *J. Geophys. Res.*, 103, 14,169–14,240, doi:10.1029/97JC02906, 1998.
- Minganti, D., Chabrillat, S., Christophe, Y., Errera, Q., Abalos, M., Prignon, M., Kinnison, D. E., and Mahieu, E.: Climatological impact of the Brewer–Dobson Circulation on the N₂O budget in WACCM, a chemical reanalysis and a CTM driven by four dynamical reanalyses, *Atmos. 860 Chem. Phys.*, 20, 12609– 12631, <https://doi.org/10.5194/acp-20-12609-2020>, 2020.
- Minganti, D., Chabrillat, S., Errera, Q., Prignon, M., Kinnison, D. E., Garcia, R. R., et al.: Evaluation of the N₂O rate of change to understand the stratospheric Brewer-Dobson Circulation in a Chemistry-Climate Model. *Journal of Geophysical Research: Atmospheres*, 127, e2021JD036390. <https://doi.org/10.1029/2021JD036390>, 2022.
- 865 Mosier, A.R., Duxbury, J.M., Freney, J.R., Heinemeyer, O. and Minami, K.: Assessing and mitigating N₂O emissions from agricultural soils, *Climatic Change*, 40, 7-38, 2000.
- Naqvi, S.W.A., Jayakumar, D.A., Narvekar, P.V., Naik, H., Sarma, V.V.S.S., D’Sousa, W., Joseph, S., and George, M.D.: Increased marine production of N₂O due to intensifying anoxia on the Indian continental shelf, *Nature*, 408, 346-349, 2000.
- 870 Nash, E.R., Newman, P.A., Rosenfield, J.E., and Schoeberl, M.R.: An objective determination of the polar vortex using Ertel's potential vorticity, *J. Geophys. Res.*, 101, 9471-9478, 1996.

- National Oceanic Atmospheric Administration (NOAA) Global Monitoring Division, Interactive Data Visualization, <https://www.esrl.noaa.gov/gmd/dv/iadv/>, accessed April 6, 2021.
- 875 Nevison, C.D., Weiss, R.F. and Erickson III, D.J.: Global Oceanic Nitrous Oxide Emissions, *J. Geophys. Res.*, 100, 15,809-15,820, 1995.
- Nevison, C.D., Kinnison, D.E. and Weiss, R.F.: Stratospheric Influence on the tropospheric seasonal cycles of nitrous oxide and chlorofluorocarbons, *Geophys. Res. Lett.* 31(20), L20103, doi:10.1029/2004GL020398, 2004.
- 880 Nevison, C.D., Keeling, R.F., Weiss, R.F., Popp, B.N., Jin, X., Fraser, P.J, Porter, L.W. and Hess, P.G.: Southern Ocean ventilation inferred from seasonal cycles of atmospheric N₂O and O₂/N₂ at Cape Grim, Tasmania, *Tellus*, 57B, 218-229, 2005.
- Nevison, C. D., Mahowald, N. M., Weiss, R.F. and Prinn, R.G.: Interannual and seasonal variability in atmospheric N₂O, *Global Biogeochem. Cy.*, 21, GB3017, doi:10.1029/2006GB002755, 2007.
- 885 Nevison, C.D., Dlugokencky, E., Dutton, G., Elkins, J.W., Fraser, P., Hall, B., Krummel, P.B., Langenfelds, R.L., O'Doherty, S., Prinn, R.G., Steele, L.P., Weiss, R.F.: Exploring causes of interannual variability in the seasonal cycles of tropospheric nitrous oxide, *Atmospheric Chemistry and Physics*, 11, doi:10.5194/acp-11-1-2011, 1-18, 2011.
- Nevison, C., Andrews, A., Thoning, K., Dlugokencky, E., Sweeney, C., Miller, S., et al.: Nitrous oxide emissions estimated with the CarbonTracker-Lagrange North American regional inversion framework. *Global Biogeochemical Cycles*, 32. <https://doi.org/10.1002/2017GB005759>, 2018.
- 890 Newman, P.: The Quasi-biennial Oscillation (QBO). Retrieved from https://acd-ext.gsfc.nasa.gov/Data_services/met/qbo/qbo.html, 2020.
- Nielsen, J.E., Pawson, S., Molod, A., Auer, B., da Silva, A.M., Douglass, A.R., et al.: Chemical mechanisms and their applications in the Goddard Earth Observing System (GEOS) Earth system model, *Journal of Advances in Modeling Earth Systems*, 9(8), 3019-3044, doi:10.1002/2017MS001011, 2017.
- 895 Olivier, J.G.J., Van Aardenne, J.A., Dentener, F., Ganzeveld, L. and Peters, W.: Recent trends in global greenhouse gas emissions: regional trends and spatial distribution of key sources. In: *Non-CO₂ Greenhouse Gases (NCGG-4)*, van Amstel, A. (coord.), page 325-330. Millpress, Rotterdam, 2005.
- 900 Park, S., et al.: Trends and seasonal cycles in the isotopic composition of nitrous oxide since 1940, *Nature Geoscience*, 5, 261-265, 2012.
- Plumb, R. A.: Stratospheric transport, *J. Meteorol. Soc. Jpn.*, 80, 793–809, 2002.
- 905 Prather, M. Hsu, J., DeLuca, N.M., Jackman, C.H., Oman, L.D., Douglass, A.R., Fleming, E.L., Strahan, S.E., Steenrod, S.D., Sovde, O.A., Isaksen, I.S.A., Froidevaux, L., Funke, B.: Measuring and modeling the lifetime of nitrous oxide including its variability, *J. Geophys. Res. Atmos.*, 120, doi:10.1002/2015JD023267, 2015.
- Prinn, R.G., Weiss, R.F., Fraser, P.J., Simmonds, P.G., Cunnold, D.M., Alyea, F.N., O'Doherty, S., Salameh, P., Miller, B.R., Huang, J., Wang, R.H.J., Hartley, D.E., Harth, C., Steele, L.P., 910 Sturrock, G., Midgley, P.M. and McCulloch, A.: A history of chemically and radiatively important gases in air deduced from ALE/GAGE/AGAGE, *J. Geophys. Res.*, 105 (D14), 17751-17792, 2000.
- Ravishankara A. R., Daniel, J. S. and Portmann, R. W.: Nitrous Oxide (N₂O): The dominant ozone

- depleting substance emitted in the 21st century, *Science*, 326,123-125, doi:
915 10.1126/science.1176985, 2009.
- Ray, E. A., Portmann, R. W., Yu, P., Daniel, J., Montzka, S. A., Dutton, G. S., et al.: The influence of the stratospheric Quasi-Biennial Oscillation on trace gas levels at the Earth's surface, *Nature Geoscience*, 13(1), 22–27. <https://doi.org/10.1038/s41561-019-0507-3>, 2020.
- Ruiz, D.J., Prather, M.J., Strahan, S.E., Thompson, R.L., Froidevaux, L., and Steenrod, S.D.: How atmospheric chemistry and transport drive surface variability of N₂O and CFC-11, *J. Geophys. Res.*, 2021.
- 920 Saikawa, E., Schlosser, C.A. and Prinn, R.G.: Global modeling of soil nitrous oxide emissions from natural processes, *Glob. Biogeochem. Cyc.*, 27, doi:[10.1002/gbc.20087](https://doi.org/10.1002/gbc.20087), 2013.
- Santoni, G. W., Daube, B. C., Kort, E. A., Jiménez, R., Park, S., Pittman, J. V., Gottlieb, E., Xiang, B., Zahniser, M. S., Nelson, D. D., McManus, J. B., Peischl, J., Ryerson, T. B., Holloway, J. S., Andrews, A. E., Sweeney, C., Hall, B., Hintsa, E. J., Moore, F. L., Elkins, J. W., Hurst, D. F., Stephens, B. B., Bent, J., and Wofsy, S. C.: Evaluation of the airborne quantum cascade laser spectrometer (QCLS) measurements of the carbon and greenhouse gas suite – CO₂, CH₄, N₂O, and CO – during the CalNex and HIPPO campaigns, *Atmos. Meas. Tech.*, 7, 1509–1526, <https://doi.org/10.5194/amt-7-1509-2014>, 2014.
- 930 Scaife, A.A. and James, I.N.: Response of the stratosphere to interannual variability of tropospheric planetary waves, *Q.J.R. Meteorol. Soc.*, 126: 275- 297, <https://doi.org/10.1002/qj.49712656214>, 2000.
- Shepherd, T. G.: Transport in the middle atmosphere, *J. Meteorol. Soc. Jpn. Ser. II*, 85, 165–191, 2007.
- 935 Sokal, R.R. and Rohlf, F.J.: *Biometry*, 859 pp., W.H. Freeman, New York, 1981.
- Stephens, B.: ORCAS Merge Products. Version 1.0, <https://doi.org/10.5065/D6SB445X>, accessed 13 Jul 2020, 2017.
- Stephens, B. B., Long, M. C., Keeling, R. F., Kort, E. A., Sweeney, C., Apel, E. C., Atlas, E. L., Beaton, S., Bent, J. D., Blake, N. J., Bresch, J. F., Casey, J., Daube, B. C., Diao, M., Diaz, E., Dierssen, H., Donets, V., Gao, B.-C., Gierach, M., Green, R., Haag, J., Hayman, M., Hills, A. J., Hoecker-Martínez, M. S., Honomichl, S. B., Hornbrook, R. S., Jensen, J. B., Li, R.-R., McCubbin, I., McKain, K., Morgan, E. J., Nolte, S., Powers, J. G., Rainwater, B., Randolph, K., Reeves, M., Schauffler, S. M., Smith, K., Smith, M., Stith, J., Stossmeister, G., Toohey, D. W., and Watt, A. S.: The O₂/N₂ Ratio and CO₂ Airborne Southern Ocean Study, *B. Am. Meteorol. Soc.*, 99, 381–402, <https://doi.org/10.1175/BAMS-D-16-0206.1>, 2018.
- 945 Stohl, A.: A 1-year Lagrangian “climatology” of airstreams in the Northern Hemisphere troposphere and lowermost stratosphere, *J. Geophys. Res.*, 106(D7), 7263–7279, 2001.
- Strahan, S. E., Oman, L.D., Douglass, A.R. and Coy, L.: Modulation of Antarctic vortex composition by the quasi-biennial oscillation, *Geophys. Res. Lett.*, 42, 4216–4223, doi:10.1002/2015GL063759, 2015.
- 950 Thompson, R.L., Dlugokencky, E., Chevallier, F., Ciais, P., Dutton, G., Langenfelds, R.L., Prinn, R.G., Weiss, R.F., Tohjima, Y., O’Doherty, S., Krummel, P.B., Fraser, P., and Steele, L.P.: Interannual variability in tropospheric nitrous oxide, 2013, *Geophys. Res. Lett.*, 40, 4426-4431, doi:10.1002/grl.50721, 2013.

- 955 Thompson, R. L., Patra, P. K., Ishijima, K., Saikawa, E., Corazza, M., Karstens, U., et al.: TransCom N₂O model inter-comparison-Part 1: Assessing the influence of transport and surface fluxes on tropospheric N₂O variability, *Atmospheric Chemistry and Physics*, 14(8), 4349–4368. <https://doi.org/10.5194/acp-14-4349-2014>, 2014a.
- 960 Thompson, R. L., Ishijima, K., Saikawa, E., Corazza, M., Karstens, U., Patra, P. K., Bergamaschi, P., Chevallier, F., Dlugokencky, E., Prinn, R. G., Weiss, R. F., O'Doherty, S., Fraser, P. J., Steele, L. P., Krummel, P. B., Vermeulen, A., Tohjima, Y., Jordan, A., Haszpra, L., Steinbacher, M., Van der Laan, S., Aalto, T., Meinhardt, F., Popa, M. E., Moncrieff, J., and P. Bousquet: TransCom N₂O model inter-comparison, Part II: Atmospheric inversion estimates of N₂O emissions, *Atmos. Chem. Phys. Discuss.*, 14, 5271–5321, doi:10.5194/acpd-14-5271-2014, 2014b.
- 965 Thompson, R.L., Lassaletta, L., Patra, P.K., Wilson, C., Wells, K.C., Gressent, A., Koffi, E.N., Chipperfield, M.P., Winiwarter, W., Davidson, E.A., Tian, H. and Canadell, J.G.: Acceleration of global N₂O emissions seen from two decades of atmospheric inversion, *Nature Climate Change*, <https://doi.org/10.1038/s41558-019-0613-7>, 2019.
- 970 Thompson, T.M., Elkins, J.W., Hall, B., Dutton, G.S., Swanson, T.H., Butler, J.H., Cummings, S.O., Fisher, D.A.: Halocarbons and other Atmospheric Trace Species, in: Schnell, R.C., A.-M. Buggle and R.M. Rosson (Eds.), *Climate Diagnostics Laboratory Summary Report #27, 2002-2003*, US Department of Commerce, National Oceanic and Atmospheric Administration, Boulder, Colorado, 2004.
- 975 Thompson, C.R., Wofsy, S.C., Prather, M.J., Newman, P.A., Hanisco, T.F., Ryerson, T.B., Fahey, D.W., Apel, E.C., Brock, C.A., Brune, W.H. et al.: The NASA Atmospheric Tomography (ATom) mission: Imaging the chemistry of the global atmosphere, *Bulletin of the American Meteorological Society*, 103 (3): E761–E790. DOI: <http://dx.doi.org/10.1175/bams-d-20-0315.1>, 2022.
- 980 Tian, H., Xu, R., Canadell, J.G., Thompson, R.L., Winiwarter, W., Suntharalingam, P., Davidson, E.A., Ciais, P., et al.: A comprehensive quantification of global nitrous oxide sources and sinks, *Nature*, 586, 248-255. <https://doi.org/10.1038/s41586-020-2780-0>, 2020.
- Volk, C.M., Elkins, J.W., Fahey, D., Dutton, G., Gilligan, J., Lowenstein, M., Podolske, J., Chan, K., and Gunson, M.: Evaluation of source gas lifetimes from stratospheric observations, *J. Geophys. Res.*, 102(D21), 25,543-25,564, 1997.
- 985 Waugh, D.W., Randel, W.J., Pawson, S., Newman, P.A. and Nash, E.R.: Persistence of the lower stratospheric polar vortices, *J. Geophys. Res.*, 104 (D22), 27,191-27,201, 1999.
- Weiss, R.F.: The temporal and spatial distribution of tropospheric nitrous oxide, *J. Geophys. Res.* 86, 7185-7195, 1981.
- 990 Wofsy, S. C., the HIPPO Science Team and Cooperating Modellers and Satellite Teams: HIAPER Pole-to-Pole Observations (HIPPO): Fine grained, global scale measurements for determining rates for transport, surface emissions, and removal of climatically important atmospheric gases and aerosols, *Phil. Trans. of the Royal Society A*, 369(1943), doi:10.1098/rsta.2010.0313, 2073-2086, 2011.

- 995 Wofsy, S., Afshar, S., Allen, H., Apel, E., Asher, E., Barletta, B., Bent, J., Bian, H., Biggs, B., Blake,
D., and et al.: ATom: Merged Atmospheric Chemistry, Trace Gases, and Aerosols,
<https://doi.org/10.3334/ORNLDAAC/1581>, accessed 13 Jul 2020, 2018.
- Wofsy, S., Daube, B., Jimenez, R., Kort, E., Pittman, J., Park, S., Commane, R., Xiang, B., Santoni, G.,
000 Jacob, D., and et al.: HIPPO Merged 10-Second Meteorology, Atmospheric Chemistry, and
Aerosol Data. Version 1.0, https://doi.org/10.3334/CDIAC/HIPPO_010, accessed 13 Jul 2020,
2017.
- WMO Greenhouse Gas Bulletin No. 14, https://library.wmo.int/doc_num.php?explnum_id=5455,
2018.
- 005 Yang, S. et al.: Global reconstruction reduces the uncertainty of oceanic nitrous oxide emissions and
reveals a vigorous seasonal cycle, *Proceedings of the National Academy of Sciences*, 117(22),
11954–11960, doi:10.1073/pnas.1921914117, 2020.